1

2 **Antagonistic relationship of NuA4 with the Non-Homologous End-Joining**

3 **machinery at DNA damage sites**

4

5

6 Salar Ahmad[1], Valerie Côté[1], Xue Cheng[1], Gaëlle Bourriquen[1], Vasileia Sapountzi[1], Mohammed

7 Altaf[1,#a] and Jacques Côté[1]*

8

9

10 [1] St-Patrick Research Group in Basic Oncology, Centre Hospitalier Universitaire de Québec-

11 Université Laval Research Center, Laval University Cancer Research Center, Quebec City, QC,

12 Canada

13 [#a] Current address: Chromatin and Epigenetics Lab, Department of Biotechnology, University of

14 Kashmir, Srinagar, Jammu and Kashmir 190006, India

15

16 * Corresponding authors: jacques.cote@crhdq.ulaval.ca (JC)

17

18 **Running Title:** NuA4 favors DNA end resection through inhibition of NHEJ factors

19

20

Abstract

The NuA4 histone acetyltransferase complex, apart from its known role in gene regulation, has also been directly implicated in the repair of DNA double-strand breaks (DSBs), favoring homologous recombination (HR) in S/G2 during the cell cycle. Here, we investigate the antagonistic relationship of NuA4 with non-homologous end joining (NHEJ) factors. We show that budding yeast Rad9, the 53BP1 ortholog, can inhibit NuA4 acetyltransferase activity when bound to chromatin *in vitro*. While we previously reported that NuA4 is recruited at DSBs during the S/G2 phase, we can also detect its recruitment in G1 when genes for NHEJ factors Rad9, Yku80 and Nej1 are mutated. This is accompanied with the binding of single-strand DNA binding protein RPA and Rad52, indicating DNA end resection in G1 as well as recruitment of the HR machinery. This NuA4 recruitment to DSBs in G1 depends on both Xrs2 and Lcd1/Ddc2. Introducing an acetyltransferase defective allele in these NHEJ mutant backgrounds decreases their hyper-resection phenotype in G1. Interestingly, we identified two novel non-histone acetylation targets of NuA4, Nej1 and Yku80. Acetyl-mimicking mutant of Nej1 inhibits repair of DNA breaks by NHEJ, decreases its interaction with other core NHEJ factors such as Yku80 and Lif1 and favors end resection. Altogether, these results establish a strong reciprocal antagonistic regulatory function of NuA4 and NHEJ factors in repair pathway choice and suggests a role of NuA4 in alternative repair mechanism that involves DNA-end resection in G1.

Author Summary

DNA double-strand breaks (DSBs) are one of the most harmful form of DNA damage. Cells employ two major repair pathways to resolve DSBs: Homologous Recombination (HR) and Non-

43 Homologous End Joining (NHEJ). Here we wanted to dissect further the role played by the NuA4
44 (Nucleosome acetyltransferase of histone H4) complex in the repair of DSBs. Budding yeast NuA4
45 complex, like its mammalian homolog TIP60 complex, has been shown to favor repair by HR.
46 Here, we show that indeed budding yeast NuA4 and components of the NHEJ repair pathway
47 share an antagonistic relationship. Deletion of NHEJ components enables increased recruitment
48 of NuA4 in the vicinity of DSBs, where NuA4 favors the end resection process which is an
49 underlying mechanism for HR repair. We also describe two independent modes responsible for
50 the recruitment of NuA4 to DSB sites. Additionally, we also present two NHEJ core components
51 as new targets of NuA4 acetyltransferase activity and suggest that these acetylation events can
52 disassemble the NHEJ repair complex from DSBs, favoring repair by HR. Our study demonstrates
53 the importance of NuA4 in the modulation of DSB repair pathway choice.
54
55

56 **Introduction**

57 The genomic integrity of a cell is under constant assault from various endogenous and exogenous
58 sources. One of the most deleterious manifestation is DNA double strand breaks (DSBs), as failure
59 to repair a DSB can lead to loss of genetic information and be an underlying cause for tumor
60 progression in higher eukaryotes (1, 2). Cells have two main pathways to repair DSBs. First,
61 Homologous Recombination (HR) is carried out in the S/G2 phase of the cell cycle, relies on 5'-3'
62 resection of the broken DNA ends and uses the homology on the sister chromatid as a template
63 for repair (3). Second, Non-Homologous End Joining (NHEJ) is carried out throughout the cell
64 cycle but it is the dominant form of repair in the G1 phase. NHEJ may or may not use processing
65 of the broken ends before ligation, making it a more error-prone pathway than HR (4). Cells also
66 have backup repair pathways such as Single Strand Annealing (SSA) and alt-NHEJ, which share
67 some components with HR and NHEJ, respectively. These pathways come into play under special
68 conditions when the main repair pathways are hindered due to genetic mutations, absence of
69 sister chromatid and state of the cell cycle (5, 6).

70 The yeast NuA4 histone acetyltransferase complex is essential for cell viability, is
71 composed of 13 subunits and is homologous to the mammalian TIP60/p400 complex (7, 8).
72 NuA4/TIP60 acetylates histones H4 and H2A N-terminal tails in chromatin, as well as variants
73 H2A.X/H2A.Z (9-13). NuA4/TIP60 has been well documented for its role in transcription
74 regulation, at the initiation and elongation steps (14, 15). NuA4 is also known to acetylate non-
75 histone proteins and regulate a variety of cellular processes such as autophagy and
76 gluconeogenesis (16, 17). Temperature sensitive mutants of Esa1, the yeast catalytic subunit, as
77 well as point mutants of H4 and H2A target lysine residues show grown defects in presence of

78 various DNA damaging chemical agents, underpinning the importance of NuA4 and acetylation
79 for the repair of DNA breaks (7, 9, 18-20). NuA4 has been shown to play an important role for the
80 recruitment of chromatin remodelers such as INO80, SWI/SNF and RSC to DNA repair sites (20-
81 22). Our recent work indicates that NuA4 is rapidly recruited to a DSB by the MRX complex
82 (Mre11-Rad50-Xrs2) and this is most likely through a DNA damage-induced phospho-dependent
83 interaction with the Xrs2 protein (23). In addition, we have shown that NuA4 directly acetylates
84 RPA to modulates its dynamic association with ssDNA during the repair process (23). NuA4 has
85 also been implicated in opposing Rad9 checkpoint activity after DNA damage in budding yeast
86 (10, 24). This is paralleled by the mammalian TIP60 complex which was shown to antagonizes
87 53BP1 (homolog of yeast Rad9) in the vicinity of DSBs to favor repair by HR (25, 26). Tip60-
88 dependant acetylation and activation of ATM has also been argued to be involved in DNA damage
89 signaling (27).

90 In this study we dissected the functional relationship of NuA4 with the NHEJ repair
91 pathway. We show that, upon removal of NHEJ factors, NuA4 is strongly recruited to DSBs during
92 the G1 phase of the cell cycle, along DNA end resection, in a Xrs2 and Lcd1/Ddc2-dependent
93 manner. Conditions of defective NuA4 acetyltransferase activity decrease the hyper-resection
94 phenotype, suggesting that NuA4 can play a role in a resection-based repair pathway in G1. In
95 addition, NHEJ core factors Nej1 and Yku80 are targets of NuA4-dependent acetylation which
96 lowers NHEJ efficiency, disrupt physical interactions and increases resection. Our results support
97 a model in which NuA4 favors repair of DSBs by resection-based pathways in part through
98 inhibition of NHEJ factors.

99

100 ## Results

101 **Deletion of NHEJ factors leads to recruitment of NuA4 at DSBs in G1**

102 Yeast Rad9, similar to its mammalian homolog 53BP1, is known to slow down or to keep a check
103 on the rate of DNA end resection (28-31). 53BP1 has been shown to have an antagonistic
104 relationship with mammalian NuA4/TIP60 (26). They compete to bind the H4K20me mark and
105 target H2AK15 modifications, implicating them in the selection of the DSB repair pathway (25).
106 In yeast, NuA4 mutant cells accumulate in the G2 phase at non-permissive temperature, in a
107 Rad9-dependent manner (10). In addition, NuA4 mutants defective in acetylation show a strongly
108 increased Rad9-dependent G1 checkpoint upon DNA damage, implicating NuA4 in an
109 antagonistic relationship with Rad9 during the DNA damage response (24).

110 Yeast Rad9 binds chromatin near DSBs through bivalent interaction with two histone
111 marks, H3K79me by its Tudor domain and H2AS129ph by its BRCT domain (γH2A) (32-34). To
112 determine if Rad9 binding to chromatin can affect NuA4 activity (Fig 1A), we performed *in vitro*
113 histone acetyltransferase (HAT) assays using native chromatin purified from cells treated with a
114 DNA damaging agent, MMS. Wild type and Tudor or BRCT mutant recombinant Rad9 (aa639-
115 1308, S1A Fig) were incubated with chromatin and purified native NuA4 complex, followed by
116 HAT assay with radioactive Acetyl-CoA. Wild type Rad9 is able to significantly block acetylation
117 of nucleosomes by NuA4, whereas Rad9-Y798Q and Rad9-K1088E are less efficient at doing so,
118 reflecting their decreased ability to bind chromatin (Fig 1B).

119 We have recently shown that NuA4 is recruited to DSBs mainly during the S/G2 phase of
120 the cell cycle (23). To study whether Rad9 may affect recruitment of NuA4 at DSBs *in vivo*, we
121 deleted *RAD9* and performed chromatin immunoprecipitations (ChIP)-qPCR at the HO-induced

122 DSB in asynchronous and G1-arrested cells. It is important to indicate all the ChIP experiments
123 presented in this study are controlled for consistent level of HO-induced DSB formation (S1D-H
124 Fig) as well as tight synchronization of cells in G1 (*bar1* mutant background, FACS and microscopic
125 analysis). While asynchronous cells show no significant difference in NuA4 binding between wild
126 type and *RAD9* deletion mutant (S1B Fig), G1 synchronized cells show a small but significant
127 increase in the recruitment of NuA4 (Fig 1C), along with the expected increase of DNA end
128 resection as measured with Rfa1, the largest subunit of RPA (Fig 1D).

129 Deletion of yeast Ku (Yku) in asynchronous cells do not significantly affect recruitment of
130 NuA4 at the HO-induced DSB (23). However, cells synchronized in G1 phase show strong
131 recruitment of NuA4 at the DSB in the absence of Yku80 (Fig 1E). ChIPs with Rfa1 also show
132 strongly increased signal for RPA around the DSB site, indicating abnormal high DNA end
133 resection in G1 (Fig 1F). We wanted to know if this antagonistic relationship was exclusive for Yku
134 or extended to other NHEJ factors. Deletion of *NEJ1*, a core NHEJ factor, in G1 synchronized cells
135 results again in increased NuA4 recruitment around the HO DSB (Fig 1G), as well as higher
136 resection (Fig 1H), which is not observed in asynchronous cells (S1C Fig).

137 In parallel, *RAD9* was deleted in the *HDF2* (*YKU80*) deleted background. Previous studies
138 have shown that the double deletion of *RAD9* and *HDF1* (*YKU70*) results in hyper-resection of
139 DNA ends at DSBs in the G1 phase of the cell cycle (35). We confirmed this finding as indicated
140 by a very strong increase of Rfa1 signal seen in *rad9*Δy*ku80*Δ cells (Fig 1F). Interestingly, a similar
141 effect is observed for NuA4, with the double deletion mutant giving a much stronger signal
142 compared to single y*ku80*Δ cells (Fig 1E). Altogether, these data demonstrate that the NuA4
143 complex can be efficiently recruited at a DSB in G1 in the absence of core NHEJ factors, Yku80

144 and Nej1, and also with the deletion of *RAD9*. This supports the concept of an antagonistic
145 relationship between NuA4 and the NHEJ machinery for repair of DNA breaks.
146
147 **Xrs2-dependent recruitment of NuA4 at DSB in G1**
148 NuA4 subunit Tra1 shows high domain homology with Tel1/ Mec1, members of the PIKK family.
149 Both Tel1 and Mec1, like their mammalian counterpart ataxia telangiectasia mutated (ATM), AT-
150 related (ATR) and DNA-dependent protein kinase (DNA-PK), are important for signaling of the
151 DSB and recruitment of downstream repair proteins (36, 37). We have recently shown that Tra1
152 gets phosphorylated upon DNA damage and its C-terminus containing the PI3K-like domain can
153 directly bind Xrs2 *in vitro*, an interaction likely involved in the recruitment of NuA4 at the HO
154 induced DSB site (23). To understand if Xrs2 is required for NuA4 recruitment at the DSB in G1,
155 we performed ChIP-qPCR in *XRS2* deletion background. As seen in (Fig 2A), the NuA4 signal
156 detected in G1 in the absence of Rad9 is completely lost when *XRS2* is deleted. The same can be
157 said for end resection measured Rfa1/RPA (Fig 2B). Strikingly, deletion of *XRS2* in the background
158 with hyper-resection (*rad9*Δy*ku80*Δ) also abrogates NuA4 recruitment and resection in G1 cells
159 (Fig 2C-D). Since deletion of *XRS2* blocks resection, it was unclear whether the loss of NuA4
160 recruitment is directly due to the loss of interaction with Xrs2 or to the loss of resection itself.
161 The *mre11-H125N* nuclease-defective mutant background was used to address this issue since it
162 is known to slow down rate of resection in G1 synchronized cells (38). As seen in (Fig 2E-F), while
163 there is a decrease in the Rfa1 signal close to the break, NuA4 detection seems unaffected. These
164 results indicate that NuA4 recruitment at a DSB in G1 requires the Xrs2 subunit of the
165 Mre11/Rad50/Xrs2 (MRX) complex.

166

167 **Lcd1/Ddc2-dependent recruitment of NuA4 at DSBs**

168 Xrs2 harbors the Nuclear Localization Sequence (NLS) required for Mre11 import into the
169 nucleus. Thus, loss of Xrs2 results in failed assembly of the MRX complex (39). To overcome this
170 issue, we used a low copy number plasmid expressing Mre11 fused to a NLS (referred to as
171 *MRE11-NLS*). In accordance with previous studies, expression of Mre11-NLS suppresses the
172 growth defect of *xrs2*Δ cells in the presence of a DNA damaging agent (MMS, S3A Fig) (39, 40).
173 Interestingly, expression of Mre11-NLS in G1 cells carrying the double deletion *rad9*Δy*ku80*Δ in
174 addition to *xrs2*Δ leads to a significant increase in NuA4 recruitment and resection (Fig 3A-B).
175 This result demonstrates an Xrs2-independent mode of NuA4 recruitment at DSBs. Importantly,
176 this Xrs2-independent mechanism is not restricted to cells in G1 as asynchronous cells also show
177 a rescue for NuA4 recruitment and resection with the introduction of *MRE11-NLS* in *xrs2*Δ cells
178 (Fig 3C-D).

179 We previously reported that the Tra1 subunit of NuA4 can interact directly with Lcd1
180 (ATRIP in mammals) *in vitro* (23). Lcd1/Ddc2 is the binding partner of Mec1 (ATR in mammals)
181 and is responsible for the recruitment of Mec1 onto the RPA-coated ssDNA generated by
182 resection (41). To establish whether NuA4 interaction with Lcd1/Ddc2 is the alternate mechanism
183 of NuA4 recruitment seen above in the absence of Xrs2, we deleted *LCD1* (in a *SML1* deleted
184 background to overcome the synthetic lethality) (42, 43). However, the introduction of *MRE11-*
185 *NLS* in this background is insufficient to rescue resection, making conclusions about NuA4
186 recruitment difficult (S3D-E Fig). To overcome this issue, we overexpressed long range resection
187 exonuclease Exo1. Expression of Mre11-NLS along with Exo1 overexpression leads to a

188 diminished DNA signal after DSB induction, indicating DNA end resection (Fig 3E)**.** This is
189 dependent on Exo1 activity since a nuclease dead mutant of the protein (Exo1-D173A) behaves
190 like the empty vector control (EV). However, in these mutant conditions allowing some DNA end
191 resection, NuA4 signals around the DSB do not change significantly in the absence of Lcd1 and
192 Xrs2 (Fig 3F). Therefore, these results support the idea that the Xrs2-independent mode of NuA4
193 recruitment at DSBs is through interaction with Lcd1/Ddc2.
194

195 **NuA4-dependent acetylation is important for hyper-resection in G1 cells**

196 DSBs flanked by direct repeats are repaired by a Rad52-dependent pathway called single strand
197 annealing (SSA). The resected ends anneal at the repeats and the intervening DNA along with one
198 repeat are removed by a nucleolytic process (44). It has been well documented that Rad52 is
199 essential for repair of DSBs by SSA in G1 cells (35). To investigate NuA4 possible function in such
200 process, we performed ChIP-qPCR to measure Rad52 recruitment to DSBs in G1 and our mutant
201 backgrounds. As expected in the hyper-resection *rad9*Δy*ku80*Δ mutant background, very high
202 recruitment of Rad52 is detected in G1 cells (Fig 4A). This is also seen in the *nej1*Δ background,
203 albeit to a lower level similar to the y*ku80*Δ single mutant (Fig 4A-B). Similar to a previous study
204 (45), we also observed recruitment of Rad51 in y*ku80*Δ and *rad9*Δy*ku80*Δ G1-blocked cells (S4A
205 Fig).

206 To determine whether NuA4 has a role in this G1 phase mechanism of DSB repair, we
207 introduced the *esa1-L254P* temperature sensitive (ts) mutant allele which affects the acetylation
208 capacity of NuA4 even at semi-restrictive temperature (as shown by western blot for the H4ac in
209 Fig 4C**)**(10). Interestingly, Rfa1 ChIP-qPCR to measure the hyper-resection phenotype in the triple

210 *rad9*Δy*ku80*Δ*esa1-ts* triple mutant background shows a significant reduction of DNA end
211 resection compared to the *rad9*Δy*ku80*Δ double mutant (Fig 4D). These results indicate that
212 NuA4 acetyltransferase activity is important to stimulate DNA end resection in G1, likely in part
213 through acetylation of chromatin in front of the resection machinery. This is supported by a
214 partial suppression of the DNA damage sensitivity of *esa1-ts* mutant cells by the *rad9*Δy*ku80*Δ
215 deletions (Fig 4E). On the other hand, we cannot observe a clear effect of NuA4 partial loss of
216 function on Rad52 recruitment in these conditions in G1 cells (S4B Fig).
217

218 **Acetylation of Nej1 by NuA4 in the regulation of DSB repair pathway choice**

219 Yeast Nej1 and its mammalian homologs XLF/NHEJ1 and PAXX have been shown to be important
220 for repair by NHEJ (46-49). Nej1 acts as a scaffolding protein for other NHEJ factors, the N-
221 terminal of Nej1 interacting with Yku and its C-terminal with Lif1 (50-52). XLF has also been shown
222 to interact with mammalian Ku and XRCC4 (50). Both Nej1 and Dnl4-Lif1 are required for
223 retention/stabilization of Yku at DSBs (45, 53). Nej1, like its mammalian homolog, is important
224 for tethering the two broken ends of the DNA (54, 55) and it was also recently shown to interact
225 with Mre11 of the MRX complex for its tethering activity (56).

226 In a large-scale *in vitro* acetylation assay on recombinant proteins, Nej1 was shown to be
227 a target of NuA4 acetyltransferase activity (17). To investigate this further and its *in vivo*
228 relevance, we purified Nej1 from yeast cells and compared the acetylated lysines detected by
229 mass spectrometry from wild type and the *esa1-L254P* NuA4 mutant backgrounds. Three lysine
230 residues, K18, K192 and K234, were detected to be acetylated on Nej1 in WT conditions but not
231 in the mutant background (S5A Fig). To determine if these acetylation sites are important for

232 Nej1 function, we produced yeast strains that express Nej1 with non-acetylatable (K to R) or
233 acetylation-mimic (K to Q) substitutions. Importantly, the point mutations do not affect the
234 stability of Nej1 (Fig 5A). Next, we tested if these lysines affect the efficiency of DSB repair by
235 NHEJ. As shown in (Fig 5B), loss of Nej1 completely abrogates repair by NHEJ, measured by re-
236 ligation efficiency for digested plasmid templates. Interestingly, both acetyl (3KQ) as well as non-
237 acetyl (3KR) substitution mutants show significantly decreased NHEJ efficiency. These results
238 demonstrate the importance of these three lysine residues in Nej1 function during DSB repair by
239 NHEJ. In contrast, Nej1 wild type and mutants show similar repair efficiency for a chromosomal
240 DSB at the *MAT* locus (S5B Fig). Importantly, ChIP-qPCRs for NuA4 and RPA around the HO-
241 induced DSB in G1 cells show significantly increased recruitment of NuA4 as well as resection in
242 the acetyl mimicking *nej1* mutant (Fig 5C-D; the non-acetyl *nej1* mutant datapoints overlap with
243 the wild type ones). The increases seen in the *nej1-3KQ* background do not reach the levels
244 obtained with the complete loss of Nej1. This could be due to Nej1-3KQ still getting recruited at
245 the break, but with impaired function. Since Nej1 interaction with other NHEJ factors is important
246 for its function (51-53, 56, 57), we performed *in vitro* protein-protein interaction analysis using
247 Nej1 mutants with Yku80 and Lif1. While wild-type Nej1 and the 3KR mutant show similar
248 interaction with Yku80, the acetyl mimicking 3KQ mutant shows less binding (Fig 5E). In parallel,
249 interaction of Nej1 with Lif1 is significantly decreased in both 3KQ and 3KR mutants compared to
250 wild type (Fig 5F). The decreased binding of Nej1-3KR with Lif1 but not with Yku80 could explain
251 its effect on the plasmid re-ligation assay (Fig 5B). Lif1 binds the Dnl4 ligase and loss of a stable
252 interaction with Nej1 may result in defective Lif1-Dnl4 recruitment, leading to impaired DSB
253 religation. However, since Nej1-3KR is still able to interact with Yku80, stabilizing it at the break,

254 it can explain the absence of effect on resection compared to wild type cells (Fig 5D).
255 Furthermore, the Nej1-3KQ acetyl-mimic mutant also shows decreased binding to the C-terminal
256 part of Mre11 compared to wild type and the 3KR mutant, which may affect its tethering activity
257 (S5D Fig). Importantly, Nej1 phosphorylation in response to DNA damaging agents (58) is not
258 affected by the 3 lysine substitutions or the depletion of NuA4 acetyltransferase activity (Esa1)
259 using the anchor-away system (59, 60)(cells are treated with DNA damaging agent MMS,
260 phosphorylation leading to the appearance of a slower migrating Nej1 signal) (S5E-G Fig).

261 In mammals, NHEJ core factor Ku70 is known to get acetylated by CBP which inhibits DNA
262 repair and regulates Bax-mediated cell apoptosis (61, 62). We tested if yeast Ku is also acetylated
263 in yeast cells and if it could be a non-histone target of NuA4, along with Nej1. Using the anchor-
264 away system to deplete Esa1 (S5G Fig) and immunoprecipitation with an anti-acetyl-lysine
265 antibody, we demonstrate that Yku80 is indeed acetylated *in vivo* and NuA4 is clearly required
266 for most of this acetylation to occur (Fig 5G). Interestingly, Yku80 acetylation seems slightly
267 higher in conditions of DNA damage. Taken together, these data indicate that Nej1 and Yku80
268 are non-histone substrates of NuA4 acetyltransferase activity. Acetylation of Nej1 may reduce
269 NHEJ efficiency by disrupting its interaction with Yku80 and Lif1. Further studies are required to
270 characterize the effect of acetylation on Yku80 function but work in higher eukaryotes also
271 supports an inhibitory role.

272

273 **Discussion**

274 Altogether, the results of this study allow us to untangle two modes of recruitment for NuA4 at
275 DSBs. The Xrs2-dependent pathway is responsible for initial recruitment of NuA4 (Fig 2), as we

276 previously reported (23). This happens early during DSB signaling and the repair process when
277 MRX is recruited to the break site. It is known that PIKK family member Tra1, subunit of NuA4,
278 can directly interact with Xrs2 (23). The other main acetyltransferase complex in yeast, SAGA,
279 also contains Tra1 and requires Xrs2 for its recruitment at the break (Cheng *et al.* unpublished).
280 Tra1 is therefore related to the Tel1(ATM) signaling kinase not only at the amino acid sequence
281 but also in its mode of recruitment at the DNA break being dependent on Xrs2 (40). Tel1 signals
282 the DSB by phosphorylation of H2A-S129 (γ-H2A) in the surrounding chromatin (63). The
283 nucleolytic processing, termed resection of the DNA breaks produces 3' ssDNA ends. This ssDNA
284 gets coated by RPA to prevent secondary structure formation and degradation. RPA-coated
285 ssDNA is recognized by various repair proteins, one such being Lcd1/Ddc2(ATRIP) (3, 41). We had
286 shown previously that Tra1 can also directly interact with Lcd1 *in vitro (23)*. Our *in vivo* data
287 support this link as NuA4 can be detected at the break in the absence of Xrs2 and this is
288 dependent on Lcd1 (Fig 3C, F and S3E Fig).

289 Resection is the event that marks the commitment of DSB repair to the HR process. The
290 3' ended ssDNA searches for the homologous sequence or sister chromatid to use as a template
291 to complete the repair process (3). Resection is a very regulated process and is active in S/G2
292 phase when the Cdk1 activity is high and inhibited during the G1 phase of the cell cycle when
293 Cdk1 activity is low (35). But it has been shown previously that resection can be achieved in G1
294 phase with the deletion of Ku protein (35, 45). In mammalian cells, HR in G1 phase requires
295 deletion of the *RAD9* homolog 53BP1, depletion of KEAP1 and a phospho-mimicking mutant of
296 CtIP (64). In our experiments we detect efficient NuA4 recruitment at a DSB in G1 concomitant
297 with the appearance of resection (Fig 1). It was previously shown that deletion of NHEJ factors in

298 G1 not only leads to resection but also repair of the DSB by SSA, relying on the recombination
299 protein Rad52 (35). Our question then was to evaluate if NuA4 played a role in this resection-
300 based repair in G1. Temperature sensitive mutant of Esa1, the catalytic subunit of NuA4, slows
301 down resection which likely impairs such repair process requiring extended end resection (Fig
302 4D). This implicates NuA4 as one of the key players in the resection-based G1 repair pathways.
303 NuA4-dependent acetylation of histone H4 and H2A tails has been shown to be important for
304 recruitment of various chromatin remodelers (INO80, SWI/SNF, RSC) and required for fidelity of
305 HR repair process (20-22). It will be interesting to verify if remodelers are also important and
306 regulated by NuA4 during repair in G1.

307 We were able to demonstrate that two NHEJ core factors, Nej1 and Yku80, are new non-
308 histone targets of NuA4 acetyltransferase activity (Fig 5G, S5A Fig). Nej1 has previous been
309 reported to be critical for NHEJ repair (46, 47, 49) and our *nej1* acetyl mutants also show impaired
310 NHEJ (Fig 5B). Nej1 is known to act as a scaffold for binding and stabilizing other proteins of the
311 NHEJ machinery (50-53). Nej1 acetyl-mimicking mutant shows reduced binding to Lif1 and Yku80
312 *in vitro*, which correlates with increased resection seen *in vivo* (Fig 5D-F). It would be interesting
313 to determine how these individual lysines affect interaction of Nej1 with other NHEJ proteins and
314 whether the tethering activity of Nej1 itself is impaired in these mutants (56). In both yeast and
315 mammals, it has been documented that Ku may interact with various histone deacetylases
316 (HDACs) and these have an important role in repair by NHEJ (65-67). Further analysis of NuA4
317 interplay with NHEJ would include identification of the specific lysines on Yku80 that get
318 acetylated by NuA4. Removal of positive charge of lysines through acetylation may reduce or
319 abrogate the binding capacity of Yku80 to DNA at the break site leading to processing/ resection

320 of the DNA ends. The acetylation may also affect the binding with Yku70 and formation of the Ku
321 complex, there by impairing NHEJ.

322 Our data supports a model (Fig 6) in which NuA4 is recruited by the MRX complex in the
323 early steps after DSB formation. Since Rad9 and other NHEJ factors get assembled at the break,
324 these, apart from inhibiting resection, may also inhibit acetylation of chromatin by NuA4. If NuA4
325 is able to directly acetylate Nej1, this blocks the assembly of the NHEJ repair machinery, thereby
326 favoring the initiation of DNA end resection. Resection then leads to RPA-coated ssDNA,
327 recruitment of Lcd1/ATRIP and subsequent NuA4 spreading away from the break, helping long-
328 range resection in the context of chromatin. Our results clearly demonstrate that NuA4 regulates
329 the repair pathway choice, away from NHEJ, and favors repair by resection-based processes
330 throughout the cell cycle. It supports and greatly broadens the conclusions of our previous work
331 that highlighted a crucial battle between 53BP1 and NuA4/TIP60 to regulate DSB repair pathway
332 choice. Future work will verify if the mammalian NuA4/ TIP60 complex also targets NHEJ proteins
333 during regulation of repair pathway choice. It is also possible that NuA4 is involved in other DSB
334 repair pathways such as alt-NHEJ, underpinning its role in resection-based repair. A better
335 understanding of how NuA4/TIP60 gets recruited to the DNA damage site and acetylates specific
336 non-histone proteins to modulate repair, identifies new molecular targets that can be acted upon
337 to treat diseases such as cancer.

338

339

340 **Methods**

341 **Yeast strains and growth assay**

342 Yeast strains used in the current study are listed in S1 Table. Standard PCR based protocol was
343 used for respective transformations employing the lithium acetate method. Yeast cells were
344 grown in YPD (1% yeast extract, 2% peptone, 2% dextrose) at 30°C or in synthetic complete
345 media. For DSB induction, cells were grown at 30 ^{o}C overnight in YP-Raffinose and 2% galactose
346 was added for 3 hours to induce HO endonuclease.

347 Yeast spot assays were performed with yeast culture grown overnight in YPD at 23°C and
348 SC-URA at 30°C, inoculated in the morning in YPD/ SC-URA at OD_{600} 0.3 and grown for 3–4 hours.
349 The 10-fold serial dilutions of the yeast cultures were made for spotting on YPD/ SC-URA plates
350 supplemented with methylmethane sulfonate (MMS). Colonies were allowed to grow for 3-4
351 days at 32°C for YPD and 30°C for SC-URA plates and the growth sensitivities were compared to
352 YPD/ SC-URA control plate.

353 **Chromatin Immunoprecipitation (ChIP)**

354 ChIP-qPCR was performed as described previously (15). In short, yeast cells were grown in YP-
355 Raff till optical density (O.D. 600) of the culture was between ~0.5 to 1. α-factor was added to
356 the indicated experiments for 6 hours to synchronize the cells in G1 phase. This was followed by
357 addition to galactose for 3 hours to induce DSB at MAT locus. Next, cells were cross-linked with
358 formaldehyde and cells were lysed by bead beating. Sonication was performed (Diagenode
359 Bioruptor) to obtain chromatin size of ~200-500 bp. 100ug of chromatin was incubated with the
360 indicated antibody overnight on a wheel at 4°C. Next day, protein A or G sephrose beads were
361 added followed by subsequent washing steps and overnight at 65°C for de-cross linking. Phenol

362 chloroform extraction was performed, and DNA samples were dissolved in NTE to be used for
363 qPCR. LC480 LightCycler (Roche) was used to quantify DNA with the primer pairs flanking the
364 indicated region left (0.15bp, 1Kb, 3Kb, 7Kb) and right (1kb, 3Kb, 7Kb) of induced DSB at MAT
365 locus. Homothallic endonuclease (HO) cutting efficiency at MAT locus was calculated using qPCR
366 with primer pair spanning the HO cut site normalized to uncut control site, interV (long intergenic
367 region on chromosome V). Primer sequences are available upon request. Antibodies used for
368 ChIP are as follows: anti-Eaf1 (7), anti-Rfa1 (Agrisera AS 07214), anti-Rad51(Santa Cruz y-180),
369 anti-Rad52(Santa Cruz yC-17).

370 **Recombinant protein purification and pull-down assay**

371 Recombinant proteins were purified from BL-21 bacteria using standard protocol described
372 previously (68). In brief, bacterial culture was growth overnight at 16°C in presence of IPTG.
373 Bacterial pellet was treated with lysozyme and sonicated. Soluble fraction was incubated with Ni-
374 nitrilotriacetic acid (NTA)-agarose (Qiagen) beads or glutathione-sepharose (GE Healthcare) for
375 3-4 hours on wheel at 4°C for His- or GST-tagged proteins respectively. Coomassie blue staining
376 was performed to estimate purified protein concentration with known bovine serum albumin
377 (BSA) standards. After elution ~300-600 ng of His-tagged protein were pre-cleared with
378 glutathione sepharose beads and incubated with immobilized GST-tagged protein in binding
379 buffer (25 mM HEPES [pH 7.5], 100 mM NaCl, 10% glycerol, 100 μg/ml BSA, 1 mM PMSF, 0.5 mM
380 dithiothreitol [DTT], 0.1% Tween 20, and protease inhibitors) at 4°C for 3 hours followed by
381 washing the beads three times. 1 μg of GST only immobilized protein was used as control. After
382 washing Laemmli buffer 1X was added followed by boiling and loading on SDS-PAGE for

383 visualization by western blotting using anti-His (Clonetech 631212) and anti-GST (Sigma G1160)
384 antibodies.

385 **Purification of acetylated Nej1 for mass spectrometry**

386 GST-tagged Nej1 was purified from wild-type and *esa1-L254P* (ts) background, followed by mass
387 spectrometry analysis to identify the acetylation sites as described previously with few
388 modifications (17). In short, cells were grown in SC-Ura containing 2% raffinose till OD_{600} ~0.8-
389 1.0. Galactose (2% final) was added for the induction of the GST-tagged Nej1 and cells were
390 grown at 37°C for two additional hours. Cells were harvested and lysed in extraction buffer
391 (10mM Tris-HCl pH 8.0, 350mM NaCl, 0.1% NP-40, 10% glycerol, 1mM DTT, 1mM PMSF, 2 µg/mL
392 leupeptin, 2 µg/mL pepstatin A, 5 µg/mL aprotinin, 5 mM β-glycerophosphate, 10 mM sodium
393 butyrate, 5 mM NaF, 10mM nicotinamide, 15µM TSA). The lysate was centrifuged at 10,000g for
394 30min at 4°C, followed by ultracentrifugation for 1 hour at 45,000g. The supernatant was
395 precleared with CL6B beads (Sigma) before the addition of glutathione-sepharose beads (GE
396 Healthcare) for 3 hours on wheel at 4°C. After binding the glutathione-sepharose beads were
397 washed 5 times with wash buffer (20mM Hepes pH7.5, 200mM NaCl, 10mM sodium butyrate).
398 Beads were mixed with elution buffer (50mM Tris-HCl pH8.0, 10mM glutathione, 10% glycerol,
399 5mM sodium butyrate) at 4°C on wheel and first elution was collected after 1 hour and other
400 after overnight incubation. Next, protein A-sepharose beads were washed with IP lysis buffer
401 (75mM Tris-HCl ph 7.5, 50mM NaCl, 1mM EDTA, 1mM EGTA, 10% glycerol, 1% Tween-20, 1mM
402 DTT, 1mM PMSF, 5mM NaF, 2 µg/mL leupeptin, 2 µg/mL pepstatin A, 5 µg/mL aprotinin, 10mM
403 sodium butyrate, 10mM, nicotinamide, 15µM TSA, 1 µM MG132) and conjugated with 6µl of
404 mouse monoclonal anti-acetylated-lysine (Cell Signalling 9681S). Antibody conjugated protein A-

405 sepharose beads were incubated with GST elution at 4°C for 3 hours on a wheel. After washing 4
406 times with IP wash buffer (50mM Hepes pH 7.0, 100mM NaCl, 10 mM sodium butyrate) 20 µl of
407 SDS-PAGE sample buffer was added and boiled. The samples were resolved by SDS-PAGE
408 followed by colloidal Coomassie blue staining to visualize and cut gel bands, which were send for
409 mass spectrometry analysis after trypsin digestion.

410 **Chromatin binding and histone acetyltransferase assay**

411 Histone acetyltransferase assay was performed as described (9, 69). 500ng of short
412 oligonucleosomes purified from methyl methanesulfonate MMS (0.05%) treated yeast cells, was
413 incubated with recombinant Rad9 at 30°C for 30 min. This was followed by the addition of NuA4
414 complex and 0.125 µCi of [^{3}H]acetyl coenzyme A ([3H]acetyl-CoA) in HAT buffer (50 mM Tris-HCl
415 [pH 8], 50 mM KCl plus NaCl, 0.1 mM EDTA, 5% glycerol, 1 mM DTT, 1 mM PMSF and 20 mM
416 sodium butyrate) at 30°C for 30 min. The reaction mixture was spotted on p81 filter paper,
417 washed and air dried. The incorporation of radiolabeled acetylation was measured by scintillation
418 counting.

419 **Non-homologous end joining (NHEJ) assay**

420 Plasmid re-ligation assay was performed as described (46). 0.4 µg plasmid pSO98 supercoiled or
421 EcoR1 digested was used to transform *nej1*Δ yeast strains that harbored wild type or mutant
422 form of the *NEJ1* gene on a CEN:ARS low copy number plasmid. The transformed yeast was plated
423 on SC-His-Leu and SC-His-Ura and kept at 30°C. After 3 days colonies were counted and ratio of
424 colonies transformed with digested plasmid to undigested supercoiled plasmid was taken. Data
425 represents two independent biological replicates and error bar denotes the range between the
426 biological replicates.

427 Chromosomal NHEJ assay was performed as described (47). Yeast background used
428 carries deletion of *HML* and *HMR* and galactose-inducible HO endonuclease that creates a single
429 DSB at the *MAT* locus. Endogenous *NEJ1* gene was deleted and wild type or mutant form of the
430 *NEJ1* gene was expressed from a low copy number CEN:ARS plasmid. The yeast cells were grown
431 overnight in YP-Raffinose media. Next day appropriate number of cells in the log phase were
432 plated on YP-Galactose and YP-Glucose plates and kept at 30°C. After 3-4 days the number of
433 colonies was quantified and ratio of colonies on YP-Galactose to YP-Glucose was calculated. Data
434 are from three independent biological replicates and error bar denotes the standard deviation
435 between the replicates.

436 **Acetyl-lysine immunoprecipitation**

437 Immunoprecipitation was performed as described previously (Cheng *et al.*, 2018). Cells were
438 grown in YPD till OD600 was ~0.5 followed by rapamycin addition (1μg/ml final) for 30 mins. MMS
439 (0.05%) or DMSO was added for 2 hours. Cells were collected and lysed in 10 mM Tris-HCl pH 8.0,
440 150 mM NaCl, 10% glycerol, 0.1% NP-40, 2 μg/mL leupeptin, 2 μg/mL pepstatin A, 5 μg/mL
441 aprotinin, 1 mM PMSF, 10 mM β-glycerophosphate, 1 mM Sodium Butyrate, 0.5 mM NaF, and 1
442 mM DTT. 4 μg of WCE was incubated with anti-acetyl (ImmuneChem ICP0380), overnight at 4°C.
443 Protein G Dynabeads (Invitrogen 10004D) was added to the reaction and kept on wheel at 4°C
444 for 4 additional hours. The IPs were washed and 1X Laemmli buffer was added and boiled. The
445 samples were resolved on SDS-PAGE followed by western blotting and analyzed with anti-Myc
446 (9E10 Babco MMS150R) and anti-Pgk1 (Abcam 113687).

447

448 ## Acknowledgments

449 We thank Olivier Jobin-Robitaille pour early work on this project, Zhiyou Deng and Yingming Zhao
450 (U. of Chicago) for mass spectrometry analysis of Nej1. We thank James E. Haber and Jennifer
451 Cobbs for stimulating discussions. We are grateful to Lorraine S. Symington for providing
452 plasmids.

453

454 ## Author contributions

455 SA, VC, XC, GB and MA performed experiments. SA and JC designed experiments, analyzed the
456 data and prepared the manuscript.

457 **Conflict of interest**

458 The authors declare that they have no conflict of interest.

459

460

461 ## References

462 1. Hanahan D, Weinberg Robert A. Hallmarks of Cancer: The Next Generation. Cell.
463 2011;144(5):646-74.
464 2. Jackson SP, Bartek J. The DNA-damage response in human biology and disease. Nature.
465 2009;461(7267):1071-8.
466 3. Symington LS. Mechanism and regulation of DNA end resection in eukaryotes. Critical
467 Reviews in Biochemistry and Molecular Biology. 2016;51(3):195-212.
468 4. Chiruvella KK, Liang Z, Wilson TE. Repair of Double-Strand Breaks by End Joining. Cold
469 Spring Harbor Perspectives in Biology. 2013;5(5).

470 5. Ceccaldi R, Rondinelli B, D'Andrea AD. Repair Pathway Choices and Consequences at the
471 Double-Strand Break. Trends in cell biology. 2016;26(1):52-64.
472 6. Bhargava R, Onyango DO, Stark JM. Regulation of Single-Strand Annealing and its Role in
473 Genome Maintenance. Trends in genetics : TIG. 2016;32(9):566-75.
474 7. Auger A, Galarneau L, Altaf M, Nourani A, Doyon Y, Utley RT, et al. Eaf1 Is the Platform for
475 NuA4 Molecular Assembly That Evolutionarily Links Chromatin Acetylation to ATP-Dependent
476 Exchange of Histone H2A Variants. Molecular and Cellular Biology. 2008;28(7):2257-70.
477 8. Doyon Y, Selleck W, Lane WS, Tan S, Côté J. Structural and Functional Conservation of the
478 NuA4 Histone Acetyltransferase Complex from Yeast to Humans. Molecular and Cellular Biology.
479 2004;24(5):1884-96.
480 9. Allard S, Utley RT, Savard J, Clarke A, Grant P, Brandl CJ, et al. NuA4, an essential
481 transcription adaptor/histone H4 acetyltransferase complex containing Esa1p and the ATM-
482 related cofactor Tra1p. The EMBO Journal. 1999;18(18):5108-19.
483 10. Clarke AS, Lowell JE, Jacobson SJ, Pillus L. Esa1p Is an Essential Histone Acetyltransferase
484 Required for Cell Cycle Progression. Molecular and Cellular Biology. 1999;19(4):2515-26.
485 11. Steunou A-L, Rossetto D, Côté J. Regulating Chromatin by Histone Acetylation. In:
486 Workman JL, Abmayr SM, editors. Fundamentals of Chromatin. New York, NY: Springer New York;
487 2014. p. 147-212.
488 12. Keogh M-C, Mennella TA, Sawa C, Berthelet S, Krogan NJ, Wolek A, et al. The
489 Saccharomyces cerevisiae histone H2A variant Htz1 is acetylated by NuA4. Genes &
490 Development. 2006;20(6):660-5.

491 13. Soria G, Polo Sophie E, Almouzni G. Prime, Repair, Restore: The Active Role of Chromatin
492 in the DNA Damage Response. Molecular Cell. 2012;46(6):722-34.
493 14. Doyon Y, Côté J. The highly conserved and multifunctional NuA4 HAT complex. Current
494 Opinion in Genetics & Development. 2004;14(2):147-54.
495 15. Rossetto D, Cramet M, Wang AY, Steunou A-L, Lacoste N, Schulze JM, et al. Eaf5/7/3 form
496 a functionally independent NuA4 submodule linked to RNA polymerase II-coupled nucleosome
497 recycling. The EMBO Journal. 2014;33(12):1397-415.
498 16. Yi C, Ma M, Ran L, Zheng J, Tong J, Zhu J, et al. Function and Molecular Mechanism of
499 Acetylation in Autophagy Regulation. Science. 2012;336(6080):474-7.
500 17. Lin Y-y, Lu J-y, Zhang J, Walter W, Dang W, Wan J, et al. Protein Acetylation Microarray
501 Reveals that NuA4 Controls Key Metabolic Target Regulating Gluconeogenesis. Cell.
502 2009;136(6):1073-84.
503 18. Choy JS, Kron SJ. NuA4 Subunit Yng2 Function in Intra-S-Phase DNA Damage Response.
504 Molecular and Cellular Biology. 2002;22(23):8215-25.
505 19. Bird AW, Yu DY, Pray-Grant MG, Qiu Q, Harmon KE, Megee PC, et al. Acetylation of histone
506 H4 by Esa1 is required for DNA double-strand break repair. Nature. 2002;419(6905):411-5.
507 20. Downs JA, Allard S, Jobin-Robitaille O, Javaheri A, Auger A, Bouchard N, et al. Binding of
508 Chromatin-Modifying Activities to Phosphorylated Histone H2A at DNA Damage Sites. Molecular
509 Cell. 2004;16(6):979-90.
510 21. Bennett G, Peterson CL. SWI/SNF recruitment to a DNA double-strand break by the NuA4
511 and Gcn5 histone acetyltransferases. DNA Repair. 2015;30:38-45.

512 22. House Nealia CM, Yang Jiahui H, Walsh Stephen C, Moy Jonathan M, Freudenreich
513 Catherine H. NuA4 Initiates Dynamic Histone H4 Acetylation to Promote High-Fidelity Sister
514 Chromatid Recombination at Postreplication Gaps. Molecular Cell. 2014;55(6):818-28.
515 23. Cheng X, Jobin-Robitaille O, Billon P, Buisson R, Niu H, Lacoste N, et al. Phospho-
516 dependent recruitment of the yeast NuA4 acetyltransferase complex by MRX at DNA breaks
517 regulates RPA dynamics during resection. Proceedings of the National Academy of Sciences.
518 2018;115(40):10028-33.
519 24. Javaheri A, Wysocki R, Jobin-Robitaille O, Altaf M, Côté J, Kron SJ. Yeast G1 DNA damage
520 checkpoint regulation by H2A phosphorylation is independent of chromatin remodeling.
521 Proceedings of the National Academy of Sciences. 2006;103(37):13771-6.
522 25. Jacquet K, Fradet-Turcotte A, Avvakumov N, Lambert J-P, Roques C, Pandita Raj K, et al.
523 The TIP60 Complex Regulates Bivalent Chromatin Recognition by 53BP1 through Direct H4K20me
524 Binding and H2AK15 Acetylation. Molecular Cell. 2016;62(3):409-21.
525 26. Tang J, Cho NW, Cui G, Manion EM, Shanbhag NM, Botuyan MV, et al. Acetylation limits
526 53BP1 association with damaged chromatin to promote homologous recombination. Nature
527 Structural & Molecular Biology. 2013;20(3):317-25.
528 27. Dantuma NP, van Attikum H. Spatiotemporal regulation of posttranslational modifications
529 in the DNA damage response. The EMBO Journal. 2016;35(1):6-23.
530 28. Ferrari M, Dibitetto D, De Gregorio G, Eapen VV, Rawal CC, Lazzaro F, et al. Functional
531 Interplay between the 53BP1-Ortholog Rad9 and the Mre11 Complex Regulates Resection, End-
532 Tethering and Repair of a Double-Strand Break. PLOS Genetics. 2015;11(1):e1004928.

533 29. Escribano-Díaz C, Orthwein A, Fradet-Turcotte A, Xing M, Young Jordan TF, Tkáč J, et al. A
534 Cell Cycle-Dependent Regulatory Circuit Composed of 53BP1-RIF1 and BRCA1-CtIP Controls DNA
535 Repair Pathway Choice. Molecular Cell. 2013;49(5):872-83.
536 30. Noordermeer SM, Adam S, Setiaputra D, Barazas M, Pettitt SJ, Ling AK, et al. The shieldin
537 complex mediates 53BP1-dependent DNA repair. Nature. 2018;560(7716):117-21.
538 31. Zimmermann M, Lottersberger F, Buonomo SB, Sfeir A, de Lange T. 53BP1 Regulates DSB
539 Repair Using Rif1 to Control 5′ End Resection. Science. 2013;339(6120):700-4.
540 32. Grenon M, Costelloe T, Jimeno S, O'Shaughnessy A, FitzGerald J, Zgheib O, et al. Docking
541 onto chromatin via the Saccharomyces cerevisiae Rad9 Tudor domain. Yeast. 2007;24(2):105-19.
542 33. Hammet A, Magill C, Heierhorst J, Jackson SP. Rad9 BRCT domain interaction with
543 phosphorylated H2AX regulates the G1 checkpoint in budding yeast. EMBO reports.
544 2007;8(9):851-7.
545 34. Wysocki R, Javaheri A, Allard S, Sha F, Côté J, Kron SJ. Role of Dot1-Dependent Histone H3
546 Methylation in G₁ and S Phase DNA Damage Checkpoint Functions of Rad9.
547 Molecular and Cellular Biology. 2005;25(19):8430-43.
548 35. Trovesi C, Falcettoni M, Lucchini G, Clerici M, Longhese MP. Distinct Cdk1 Requirements
549 during Single-Strand Annealing, Noncrossover, and Crossover Recombination. PLOS Genetics.
550 2011;7(8):e1002263.
551 36. Abraham RT. Cell cycle checkpoint signaling through the ATM and ATR kinases. Genes &
552 Development. 2001;15(17):2177-96.
553 37. Smith GCM, Jackson SP. The DNA-dependent protein kinase. Genes & Development.
554 1999;13(8):916-34.

555 38. Clerici M, Mantiero D, Guerini I, Lucchini G, Longhese MP. The Yku70–Yku80 complex
556 contributes to regulate double-strand break processing and checkpoint activation during the cell
557 cycle. EMBO reports. 2008;9(8):810-8.
558 39. Tsukamoto Y, Mitsuoka C, Terasawa M, Ogawa H, Ogawa T. Xrs2p Regulates Mre11p
559 Translocation to the Nucleus and Plays a Role in Telomere Elongation and Meiotic
560 Recombination. Molecular Biology of the Cell. 2005;16(2):597-608.
561 40. Oh J, Al-Zain A, Cannavo E, Cejka P, Symington Lorraine S. Xrs2 Dependent and
562 Independent Functions of the Mre11-Rad50 Complex. Molecular Cell. 2016;64(2):405-15.
563 41. Zou L, Elledge SJ. Sensing DNA Damage Through ATRIP Recognition of RPA-ssDNA
564 Complexes. Science. 2003;300(5625):1542-8.
565 42. Gobbini E, Cesena D, Galbiati A, Lockhart A, Longhese MP. Interplays between ATM/Tel1
566 and ATR/Mec1 in sensing and signaling DNA double-strand breaks. DNA Repair. 2013;12(10):791-
567 9.
568 43. Paciotti V, Clerici M, Lucchini G, Longhese MP. The checkpoint protein Ddc2, functionally
569 related to S. pombe Rad26, interacts with Mec1 and is regulated by Mec1-dependent
570 phosphorylation in budding yeast. Genes & Development. 2000;14(16):2046-59.
571 44. Ivanov EL, Sugawara N, Fishman-Lobell J, Haber JE. Genetic Requirements for the Single-
572 Strand Annealing Pathway of Double-Strand Break Repair in Saccharomyces
573 cerevisiae. Genetics. 1996;142(3):693-704.
574 45. Zhang Y, Hefferin ML, Chen L, Shim EY, Tseng H-M, Kwon Y, et al. Role of Dnl4–Lif1 in
575 nonhomologous end-joining repair complex assembly and suppression of homologous
576 recombination. Nature Structural & Molecular Biology. 2007;14(7):639-46.

577 46. Ooi SL, Shoemaker DD, Boeke JD. A DNA Microarray-Based Genetic Screen for
578 Nonhomologous End-Joining Mutants in Saccharomyces cerevisiae. Science.
579 2001;294(5551):2552-6.
580 47. Valencia M, Bentele M, Vaze MB, Herrmann G, Kraus E, Lee SE, et al. NEJ1 controls non-
581 homologous end joining in Saccharomyces cerevisiae. Nature. 2001;414(6864):666-9.
582 48. Chang HHY, Pannunzio NR, Adachi N, Lieber MR. Non-homologous DNA end joining and
583 alternative pathways to double-strand break repair. Nature Reviews Molecular Cell Biology.
584 2017;18(8):495-506.
585 49. Kegel A, Sjöstrand JOO, Åström SU. Nej1p, a cell type-specific regulator of
586 nonhomologous end joining in yeast. Current Biology. 2001;11(20):1611-7.
587 50. Deshpande RA, Wilson TE. Modes of interaction among yeast Nej1, Lif1 and Dnl4 proteins
588 and comparison to human XLF, XRCC4 and Lig4. DNA repair. 2007;6(10):1507-16.
589 51. Sulek M, Yarrington R, McGibbon G, Boeke JD, Junop M. A critical role for the C-terminus
590 of Nej1 protein in Lif1p association, DNA binding and non-homologous end-joining. DNA Repair.
591 2007;6(12):1805-18.
592 52. Mahaney BL, Lees-Miller SP, Cobb JA. The C-terminus of Nej1 is critical for nuclear
593 localization and non-homologous end-joining. DNA Repair. 2014;14:9-16.
594 53. Chen X, Tomkinson AE. Yeast Nej1 Is a Key Participant in the Initial End Binding and Final
595 Ligation Steps of Nonhomologous End Joining. Journal of Biological Chemistry. 2011;286(6):4931-
596 40.

597 54. Reid DA, Keegan S, Leo-Macias A, Watanabe G, Strande NT, Chang HH, et al. Organization
598 and dynamics of the nonhomologous end-joining machinery during DNA double-strand break
599 repair. Proceedings of the National Academy of Sciences. 2015;112(20):E2575-E84.
600 55. Graham TGW, Carney SM, Walter JC, Loparo JJ. A single XLF dimer bridges DNA ends
601 during nonhomologous end joining. Nature Structural & Molecular Biology. 2018;25(9):877-84.
602 56. Mojumdar A, Sorenson K, Hohl M, Toulouze M, Lees-Miller SP, Dubrana K, et al. Nej1
603 Interacts with Mre11 to Regulate Tethering and Dna2 Binding at DNA Double-Strand Breaks. Cell
604 Reports. 2019;28(6):1564-73.e3.
605 57. Sorenson KS, Mahaney BL, Lees-Miller SP, Cobb JA. The non-homologous end-joining
606 factor Nej1 inhibits resection mediated by Dna2–Sgs1 nuclease-helicase at DNA double strand
607 breaks. Journal of Biological Chemistry. 2017;292(35):14576-86.
608 58. Ahnesorg P, Jackson SP. The non-homologous end-joining protein Nej1p is a target of the
609 DNA damage checkpoint. DNA Repair. 2007;6(2):190-201.
610 59. Haruki H, Nishikawa J, Laemmli UK. The Anchor-Away Technique: Rapid, Conditional
611 Establishment of Yeast Mutant Phenotypes. Molecular Cell. 2008;31(6):925-32.
612 60. Kollenstart L, de Groot AJL, Janssen GMC, Cheng X, Vreeken K, Martino F, et al. Gcn5 and
613 Esa1 function as histone crotonyltransferases to regulate crotonylation-dependent transcription.
614 Journal of Biological Chemistry. 2019;294(52):20122-34.
615 61. Cohen HY, Lavu S, Bitterman KJ, Hekking B, Imahiyerobo TA, Miller C, et al. Acetylation of
616 the C Terminus of Ku70 by CBP and PCAF Controls Bax-Mediated Apoptosis. Molecular Cell.
617 2004;13(5):627-38.

618 62. Li S, Shi B, Liu X, An H-X. Acetylation and Deacetylation of DNA Repair Proteins in Cancers.
619 Frontiers in Oncology. 2020;10(2184).
620 63. Harrison JC, Haber JE. Surviving the Breakup: The DNA Damage Checkpoint. Annual
621 Review of Genetics. 2006;40(1):209-35.
622 64. Orthwein A, Noordermeer SM, Wilson MD, Landry S, Enchev RI, Sherker A, et al. A
623 mechanism for the suppression of homologous recombination in G1 cells. Nature.
624 2015;528(7582):422-6.
625 65. Jeong J, Juhn K, Lee H, Kim S-H, Min B-H, Lee K-M, et al. SIRT1 promotes DNA repair activity
626 and deacetylation of Ku70. Experimental & Molecular Medicine. 2007;39(1):8-13.
627 66. Miller KM, Tjeertes JV, Coates J, Legube G, Polo SE, Britton S, et al. Human HDAC1 and
628 HDAC2 function in the DNA-damage response to promote DNA nonhomologous end-joining.
629 Nature Structural & Molecular Biology. 2010;17(9):1144-51.
630 67. Boulton SJ, Jackson SP. Components of the Ku-dependent non-homologous end-joining
631 pathway are involved in telomeric length maintenance and telomeric silencing. The EMBO
632 Journal. 1998;17(6):1819-28.
633 68. Setiaputra D, Ahmad S, Dalwadi U, Steunou A-L, Lu S, Ross JD, et al. Molecular
634 Architecture of the Essential Yeast Histone Acetyltransferase Complex NuA4 Redefines Its
635 Multimodularity. Molecular and Cellular Biology. 2018;38(9):e00570-17.
636 69. Steunou A-L, Cramet M, Rossetto D, Aristizabal MJ, Lacoste N, Drouin S, et al. Combined
637 Action of Histone Reader Modules Regulates NuA4 Local Acetyltransferase Function but Not Its
638 Recruitment on the Genome. Molecular and Cellular Biology. 2016;36(22):2768-81.

639 70. Lee SE, Moore JK, Holmes A, Umezu K, Kolodner RD, Haber JE. Saccharomyces Ku70,
640 Mre11/Rad50, and RPA Proteins Regulate Adaptation to G2/M Arrest after DNA Damage. Cell.
641 1998;94(3):399-409.

642

643

644 **FIGURE LEGENDS:**

645 **Fig 1: NHEJ factors inhibit NuA4 recruitment and end resection at a DSB in G1.**

646 (A) Schematic representation of Fig1B, wild type Rad9 binds to chromatin and inhibits NuA4 from
647 acetylating histones, whereas Rad9 mutants are unable to bind chromatin thus resulting in
648 acetylation of histones by NuA4.

649 (B) *In vitro* HAT assay showing inhibition of NuA4 acetyltransferase activity by Rad9 using yeast
650 native chromatin and recombinant Rad9 (wild type, tudor-Y798Q and BRCT- K1088E domain
651 mutant). Recombinant Rad9 wild type and mutants were incubated with MMS-treated purified
652 yeast native chromatin. Afterwards NuA4 was added along with ^{3}H-acetyl-CoA followed by
653 spotting on P81 membrane and scintillation counting. Error bars indicate the ranges of duplicate
654 reactions.

655 (C-H) ChIP-qPCR showing increased recruitment of NuA4(Eaf1 subunit) and Rfa1 (RPA) in *rad9*Δ
656 (C-D)*, yku80*Δ, y*ku80*Δ*rad9*Δ (E-F) and *nej1*Δ (G-H) compared to wild type at an HO-induced DSB
657 in G1. ChIP-qPCR analysis was performed using Eaf1 and Rfa1 antibodies. Cells with *bar1*Δ
658 background were synchronized in G1 phase using α-factor for 6 hours in YP-Raffinose followed
659 by addition of galactose for 3 hours to induce DSB. The data represents two independent
660 biological replicates and error bar denotes range between the replicates. Yeast strains used had
661 similar HO cutting efficiency (S1D-H Fig)

662

663 **Fig 2: Xrs2-dependent recruitment of NuA4 at a DSB in G1.**

664 (A-D) ChIP-qPCR of Rfa1 and Eaf1 shows loss of NuA4 (A, C) and resection (B, D) in *xrs2*Δ,
665 *xrs2*Δ*rad9*Δ (A-B) and *xrs2*Δ*rad9*Δy*ku80*Δ (D-E) compared to wild type at HO-induced DSB in G1
666 synchronized cells.
667 (E-F) ChIP-qPCR in the *mre11-H125N* mutant shows decreased resection but unaffected NuA4
668 recruitment compared to wild type in G1 cells. ChIP-qPCR was performed as described in (Fig 1).
669 Yeast strains used showed similar HO cutting efficiency (S2A-C Fig).
670
671 **Fig 3: Xrs2-independent and Lcd1-dependent recruitment of NuA4 at DSB.**
672 (A-D) Resection and NuA4 recruitment is restored in *xrs2*Δ background with expression of Mre11-
673 NLS from a low copy number CEN:ARS plasmid. ChIP-qPCR of Eaf1 and Rfa1 was performed as in
674 (Fig 1). (A-B) In G1 cells the increase in NuA4 and Rfa1 is seen in the *rad9*Δy*ku80*Δ background.
675 (C-D) In asynchronous cells; expression of Mre11-NLS is enough to restore NuA4 and Rfa1 levels
676 comparable to WT on the left side proximal to the DSB site.
677 (E-F) NuA4 recruitment to DSB requires Lcd1. (E) Resection is rescued in *lcd1*Δ*xrs2*Δ+*pMRE11-*
678 *NLS* with overexpression of Exo1-WT but not Exo1-D173A mutant. (F) NuA4 signal does not show
679 a resection-correlated increase with Exo1-WT compared to the Exo1-D173A mutant or the empty
680 vector. % of Intact DNA was determined by qPCR on genomic DNA at indicated sites and
681 normalized to negative control intergenic V. Cells were grown in YP-Raff till early log phase
682 followed by addition of galactose for 3 hours to induce the DSB. Yeast strains used had similar
683 HO cutting efficiency (S3B, C, F Fig).
684
685 **Fig 4: Decreased hyper-resection in *esa1* temperature sensitive mutant in G1.**

686 (A-B) ChIP-qPCR of Rad52 around HO-induced DSB in G1 blocked cells. *rad9*Δy*ku80*Δ, y*ku80*Δ (A)
687 and *nej1*Δ (B) show higher recruitment of Rad52 than compared to wild type.
688 (C) Reduced histone H4 acetylation in *esa1-ts* background at semi-restrictive temperature.
689 Western blot analysis for WCE of yeast strains used for ChIP-qPCR in (D). Samples were collected
690 before addition of α-factor at permissive temperature (23°C) in YP-Raff. α-factor was added and
691 cultures were moved to semi-restrictive temperature (32°C) followed by addition of galactose to
692 induced DSB for 3 hours.
693 (D) ChIP-qPCR of Rfa1 around the HO-induced DSB in G1 cells showing reduced resection in
694 *rad9Δyku80Δ* background with the introduction of the *esa1-ts* NuA4 defective allele. Yeast strains
695 used had similar HO cutting efficiency (S4C Fig).
696 (E) The sensitivity of the *esa1-ts* mutant cells to DNA damage is partially suppressed by deletion
697 of core NHEJ factors. 10-fold serial dilution spot assays were performed with *esa1-L254P*,
698 *rad9*Δy*ku80*Δ and *rad9*Δy*ku80*Δ*esa1-L254P* cells in the absence or the presence of DNA damaging
699 agent MMS.
700
701 **Fig 5: NuA4 inhibits NHEJ through acetylation of Nej1.**
702 (A) Western blot on whole cell extracts comparing wild type and mutant Nej1 expression levels
703 in strains used in (B).
704 (B) *nej1-3KR* and *nej1-3KQ* mutant cells show reduced plasmid re-ligation efficiency for EcoR1
705 linearized pSO98 plasmid. Samples were normalized to wild type, which was set at 100%.
706 (C-D) Increased NuA4 and resection/RPA recruitment in the *nej1-3KQ* mutant compared to wild
707 type *NEJ1* and the *nej1-3KR* mutant background. ChIP-qPCR using anti-Eaf1 (D) and anti-Rfa1 (E)

708 antibodies in G1 synchronized cells as described in (Fig 1). Yeast strains used showed similar HO
709 cutting efficiency (S5C Fig).
710 (E) Recombinant Nej1-3KQ shows reduced interaction with rKu80 compared to Nej1-WT and
711 Nej1-3KR. rNej1 is GST tagged for pull-down whereas rKu80 is 6X-His tagged. Empty GST was used
712 as negative control.
713 (F) Recombinant Nej1-3KQ and Nej1-3KR show reduced interaction with rLif1 compared to wild
714 type Nej1. rLif1 is 6X-His tagged. Empty GST was used as negative control.
715 (G) Ku80 is acetylated on lysine residues *in vivo* in a NuA4-dependent manner. Acetyl-lysine
716 immunoprecipitation in an Esa1-FRB anchor away/Yku80-13myc background shows much
717 reduced signal for Yku80 after the rapamycin treatment that depletes Esa1 from the nucleus. The
718 effect of DNA damage was also monitored by treating the cells with MMS. Pgk1 was used as
719 loading control. The efficiency of Esa1 depletion was monitored by western blot showing loss of
720 H4 acetylation (S5G Fig).
721
722 **Fig 6: NuA4 regulates DSB repair pathway choice, favoring resection-based repair.**
723 While chromatin-bound Rad9 can inhibit NuA4-dependent acetylation to favor repair by NHEJ,
724 NuA4 regulates DSB repair pathway choice by acetylating NHEJ core factors like Nej1 and Yku80.
725 This perturbs the interaction between NHEJ factors, enabling resection of DNA ends. As resection
726 produces ssDNA more NuA4 is recruited through its interaction with Lcd1/Ddc2. “Ac” represents
727 acetylation performed by NuA4.
728
729

730 **Supporting Information:**

731 **S1 Fig. NuA4 and resection spreading are not inhibited by NHEJ factors in asynchronous cells.**

732 (A) Purified recombinant Rad9 wild-type and mutants were resolved by SDS-PAGE and stained
733 with Coomassie blue stain. Known concentrations of BSA were used to estimation the
734 concentration of purified recombinant proteins using ImageJ software.

735 (B) ChIP-qPCR showing NuA4 enrichment around DSB at *MAT* locus between wild type and *rad9*Δ
736 in asynchronous cells.

737 (C) ChIP-qPCR with antibody against Rfa1 showing no difference in resection at *MAT* locus
738 between wild type and *nej1*Δ in asynchronous cells.

739 (D-H) HO cutting efficiency at *MAT* locus after 3 hours of galactose induction between wild type
740 and, *rad9*Δ asynchronous cells (C), *rad9*Δ G1 synchronized cells (D), y*ku80*Δ and y*ku80*Δ*rad9*Δ G1
741 synchronized cells (E), *nej1*Δ G1 synchronized cells (F), *nej1*Δ asynchronous cells (G).

742

743 **S2 Fig. Difference in NuA4 and resection signal seen between wild type and mutants not caused**
744 **by uneven HO cutting at *MAT* locus.**

745 (A-C) HO cutting efficiency at MAT locus in G1 synchronized cells after 3 hours of galactose
746 induction between wild type and, *xrs2*Δ*rad9*Δ (A), *xrs2*Δ*rad9*Δy*ku80*Δ (B), *mre11-H125N* (C).

747

748 **S3 Fig. *MRE11-NLS* suppresses defect of *xrs2*Δ.**

749 (A) Phenotypic analysis showing introduction of *MRE11-NLS* suppresses the sensitivity of *xrs2*Δ
750 to DNA damaging drug, MMS. 1:10 serial dilutions of log phase cells were spotted on synthetic
751 complete -URA plates with and without MMS.

752 (B-C) HO cutting efficiency at *MAT* locus after 3 hours of galactose induction in the indicated
753 strains.
754 (D-E) ChIP-qPCR showing *lcd1*Δ *xrs2*Δ results in loss of RPA signal (D), and loss of NuA4 (E) at HO
755 induced DSB at *MAT* locus in asynchronous cells. *lcd1*Δ (loss of Mec1) does not affect resection
756 but shows less signal compared to wild type near the break.
757 (F) HO cutting efficiency at *MAT* locus after 3 hours of galactose induction in the indicated strains.
758
759 **S4 Fig. *esa1-ts* does not affect the recruitment of recombination protein in hyper resection**
760 **background in G1 phase.**
761 (A) ChIP-qPCR with Rad51 antibody around the induced DSB at *MAT* locus in G1 synchronized
762 cells. y*ku80*Δ and y*ku80*Δ*rad9*Δ show higher signal compared to wild type.
763 (B) ChIP-qPCR with Rad52 antibody around the induced DSB at *MAT* locus in G1 synchronized
764 cells. *rad9Δyku80Δ* and *rad9Δyku80Δesa1-ts* show higher signal for Rad52 than wild type.
765 (C) HO cutting efficiency in wild type, *rad9Δyku80Δ* and *rad9Δyku80Δesa1-ts* at *MAT* locus in G1
766 synchronized cells after 3 hours of galactose induction.
767
768 **S5 Fig. Nej1 mutants do not disrupt DNA damage induced phosphorylation but affect binding**
769 **to Mre11.**
770 (A) Nej1 is acetylated *in vivo* on residues K18, K192 and K234 in a NuA4-dependent manner. Mass
771 spectrometry analysis of Nej1 lysine acetylation sites in *ESA1* wild type and temperature sensitive
772 (ts) mutant.

773 (B) Nej1 wild-type and lysine mutants show similar ability to repair chromosomal DSB induced at
774 *MAT* locus by HO induction.
775 (C) HO cutting efficiency at *MAT* locus in G1 synchronized cells after 3 hours of galactose
776 induction in the indicated *nej1*Δ strains.
777 (D) *In vitro* protein pull-down assay showing recombinant Nej1 wild type and Nej1-3KR binds to
778 C-terminal of rMre11, while this interaction is much reduced with Nej1-3KQ. Empty GST was used
779 as negative control.
780 (E) Nej1 lysine mutants do not affect the DNA damage induced phosphorylation of Nej1. Western
781 blot analysis of whole cell extracts (WCE) prepared from indicated yeast strains treated with MMS
782 (0.05%) or DMSO (control) for 2 hours. Pgk1 was used as loading control.
783 (F) Western blot analysis on WCE showing depletion of Esa1 does not affect the DNA damage
784 induced phosphorylation of Nej1. Esa1 was FRB tagged and depleted from the nucleus using the
785 anchor away system in presence of rapamycin. This was followed by treatment of cells with MMS
786 or DMSO. Pgk1 was used as loading control.
787 (G) Western blot analysis of yeast WCE showing reduced acetylation of H4 in the anchor away
788 background with Esa1 FRB tagged after rapamycin treatment. H2B was used as loading control.
789
790

791 **S1 Table: Yeast strains used in the current study**

Strain	Genotype	Reference
JKM139	*MATa hoΔ hmlΔ::ADE1 hmrΔ::ADE1 ade1-100 leu2-3;112 lys5 trp1::hisG ura3-52 ade3::GAL-HO*	(70)
QY2211	JKM139 *bar1Δ::NATMX*	This study
QY2212	JKM139 *bar1Δ::NATMX rad9Δ::KANMX*	This study
QY2213	JKM139 *bar1Δ::NATMX yku80Δ::TRP1*	This study
QY2214	JKM139 *bar1Δ::NATMX rad9Δ::KANMX yku80Δ::TRP1*	This study
QY2231	JKM139 *bar1Δ::LEU2 rad9Δ::KANMX yku80Δ::TRP1 esa1-L254P::NATMX*	This study
QY2215	JKM139 *bar1Δ::NATMX nej1Δ::TRP1*	This study
QY2216	JKM139 *bar1Δ::NATMX xrs2Δ::TRP1*	This study
QY2217	JKM139 *bar1Δ::NATMX rad9Δ::KANMX xrs2Δ::TRP1*	This study
QY2218	JKM139 *bar1Δ::NATMX rad9Δ::KANMX xrs2Δ::TRP1 yku80Δ::HPHMX*	This study
QY2219	JKM139 *bar1Δ::NATMX mre11-H125N::HPHMX*	This study
QY2220	JKM139 *bar1Δ::NATMX* + (pRS416)	This study
QY2221	JKM139 *bar1Δ::NATMX xrs2Δ::TRP1* + (pRS416)	This study
QY2222	JKM139 *bar1Δ::NATMX xrs2Δ::TRP1* + (pRS416 *MRE11-NLS*)	This study
QY2223	JKM139 *bar1Δ::NATMX rad9Δ::KANMX xrs2Δ::TRP1 yku80Δ::HPHMX* + (pRS416 *MRE11-NLS*)	This study

QY1603	JKM139 *sml1::NATMX*	(23)
QY1604	JKM139 *sml1::NATMX lcd1::KANMX*	(23)
QY2224	QY1603 + (pRS416)	This study
QY2225	QY1604 + (pRS416)	This study
QY-2226	QY1604 *xrs2Δ::LEU2* + (pRS416)	This study
QY2227	QY1604 *xrs2Δ::LEU2* + (pRS416 *MRE11-NLS*)	This study
QY2228	QY2227 + (pRS424 *TRP1 2μ ori*)	This study
QY2229	QY2227 + (pRS424 *EXO1 TRP1 2μ ori*)	This study
QY2230	QY2227 + (pRS424 *EXO1-D173A TRP1 2μ ori*)	This study
QY2600	BY4741 *MATa his3Δ1 leu2Δ0 met15Δ0 ura3Δ0 nej1Δ*::*KANMX*	This study
QY2232	QY2600 + (pRS413)	This study
QY2233	QY2600 + (pRS413 *NEJ1*)	This study
QY2234	QY2600 + (pRS413 *NEJ1-K18R-K192R-K234R*)	This study
QY2235	QY2600 + (pRS413 *NEJ1-K18Q-K192Q-K234Q*)	This study
QY2236	QY2215 + (pRS416)	This study
QY2237	QY2215 + (pRS416 *NEJ1*)	This study
QY2238	QY2215 + (pRS416 *NEJ1-K18R-K192R-K234R*)	This study
QY2239	QY2215 + (pRS416 *NEJ1-K18Q-K192Q-K234Q)*	This study
QY3572	JKM139 *fpr1Δ::HphMX tor1-1::URA3 RPL13A-2*FKBP12::TRP1 FRB-ESA1::KanMX*	(60)
QY2240	QY3572 *YKU80-13MYC::NATMX*	This study

QY2241	QY3572 *NEJ1-13MYC::NATMX*	This study
QY2054	BY4741 *MATa his3Δ1 leu2Δ0 met15Δ0 ura3Δ0* +pEGH(GAL-GST-Nej1)	Open Biosystem
QY2058	BY4741 *MATa his3Δ1 leu2Δ0 met15Δ0 ura3Δ0 esa1Δ::KanMX* +pSAPE5(HA-*esa1-L254P LEU2 ARS/CEN*) +pEGH(GAL-GST-Nej1)	This study

792

FIGURE 1

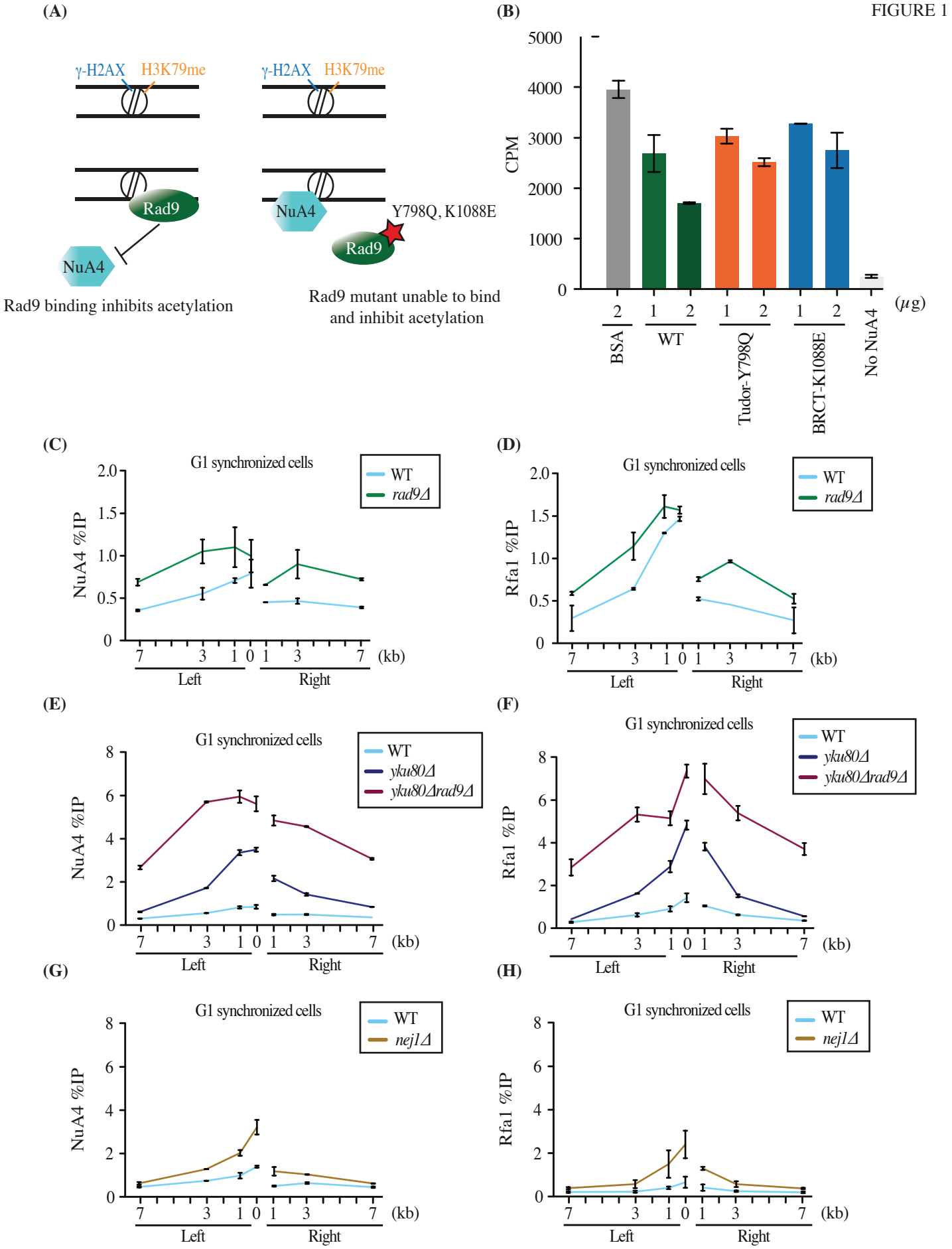
(A)
γ-H2AX
H3K79me
Rad9
NuA4
Rad9 binding inhibits acetylation
γ-H2AX
H3K79me
NuA4
Y798Q, K1088E
Rad9
Rad9 mutant unable to bind and inhibit acetylation
(B)
CPM
5000
4000
3000
2000
1000
0
2 1 2 1 2 1 2
(μg)
BSA
WT
Tudor-Y798Q
BRCT-K1088E
No NuA4
(C)
G1 synchronized cells
WT
rad9Δ
NuA4 %IP
2.0
1.5
1.0
0.5
0
7 3 1 0 1 3 7 (kb)
Left
Right
(D)
G1 synchronized cells
WT
rad9Δ
Rfa1 %IP
2.0
1.5
1.0
0.5
0
7 3 1 0 1 3 7 (kb)
Left
Right
(E)
G1 synchronized cells
WT
yku80Δ
yku80Δrad9Δ
NuA4 %IP
8
6
4
2
0
7 3 1 0 1 3 7 (kb)
Left
Right
(F)
G1 synchronized cells
WT
yku80Δ
yku80Δrad9Δ
Rfa1 %IP
8
6
4
2
0
7 3 1 0 1 3 7 (kb)
Left
Right
(G)
G1 synchronized cells
WT
nej1Δ
NuA4 %IP
8
6
4
2
0
7 3 1 0 1 3 7 (kb)
Left
Right
(H)
G1 synchronized cells
WT
nej1Δ
Rfa1 %IP
8
6
4
2
0
7 3 1 0 1 3 7 (kb)
Left
Right

FIGURE 2

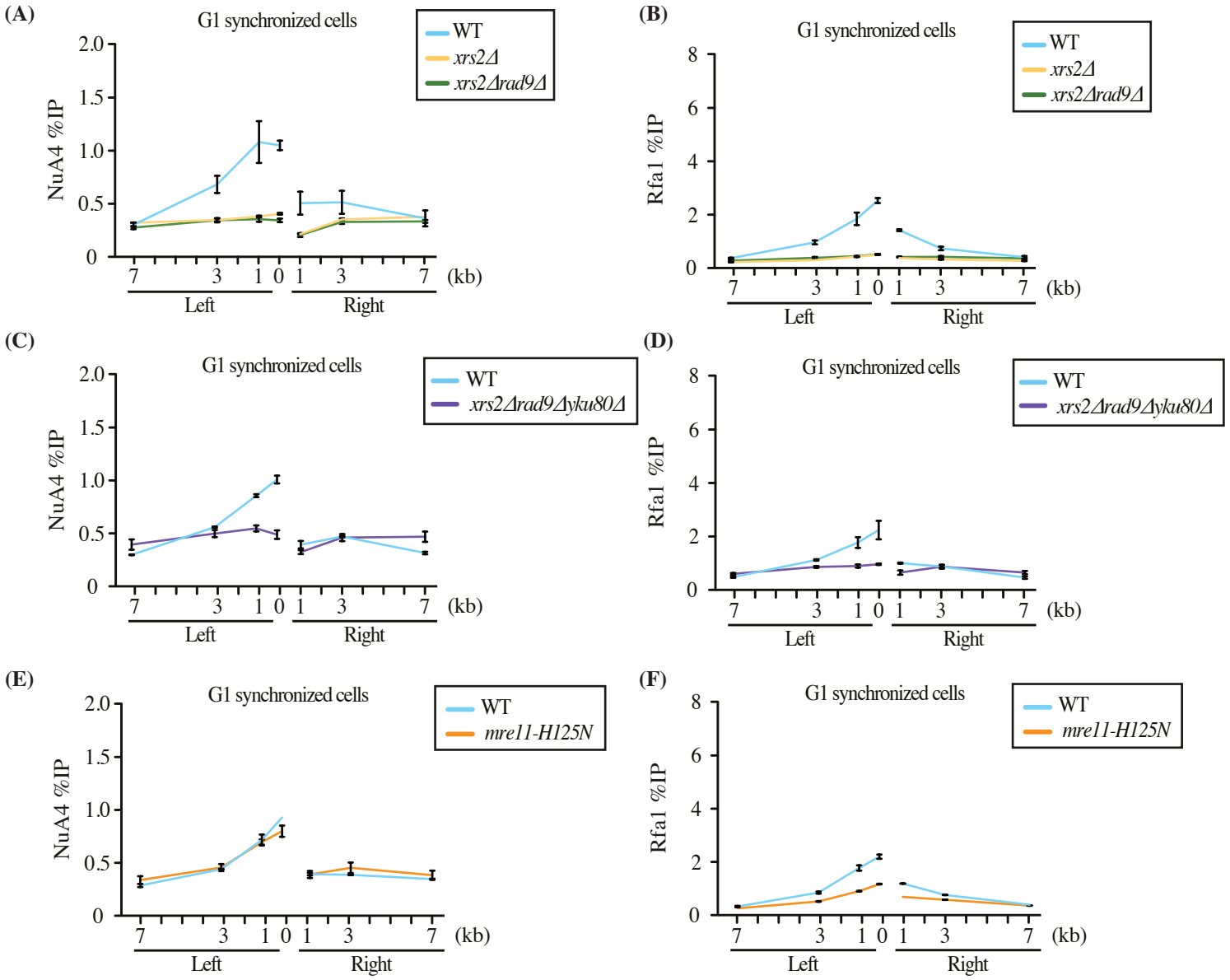
(A)
G1 synchronized cells
WT
xrs2Δ
xrs2Δrad9Δ
NuA4 %IP
2.0
1.5
1.0
0.5
0
7
3
1
0
1
3
7
(kb)
Left
Right
(B)
G1 synchronized cells
WT
xrs2Δ
xrs2Δrad9Δ
Rfa1 %IP
8
6
4
2
0
7
3
1
0
1
3
7
(kb)
Left
Right
(C)
G1 synchronized cells
WT
xrs2Δrad9Δyku80Δ
NuA4 %IP
2.0
1.5
1.0
0.5
0
7
3
1
0
1
3
7
(kb)
Left
Right
(D)
G1 synchronized cells
WT
xrs2Δrad9Δyku80Δ
Rfa1 %IP
8
6
4
2
0
7
3
1
0
1
3
7
(kb)
Left
Right
(E)
G1 synchronized cells
WT
mre11-H125N
NuA4 %IP
2.0
1.5
1.0
0.5
0
7
3
1
0
1
3
7
(kb)
Left
Right
(F)
G1 synchronized cells
WT
mre11-H125N
Rfa1 %IP
8
6
4
2
0
7
3
1
0
1
3
7
(kb)
Left
Right

FIGURE 3

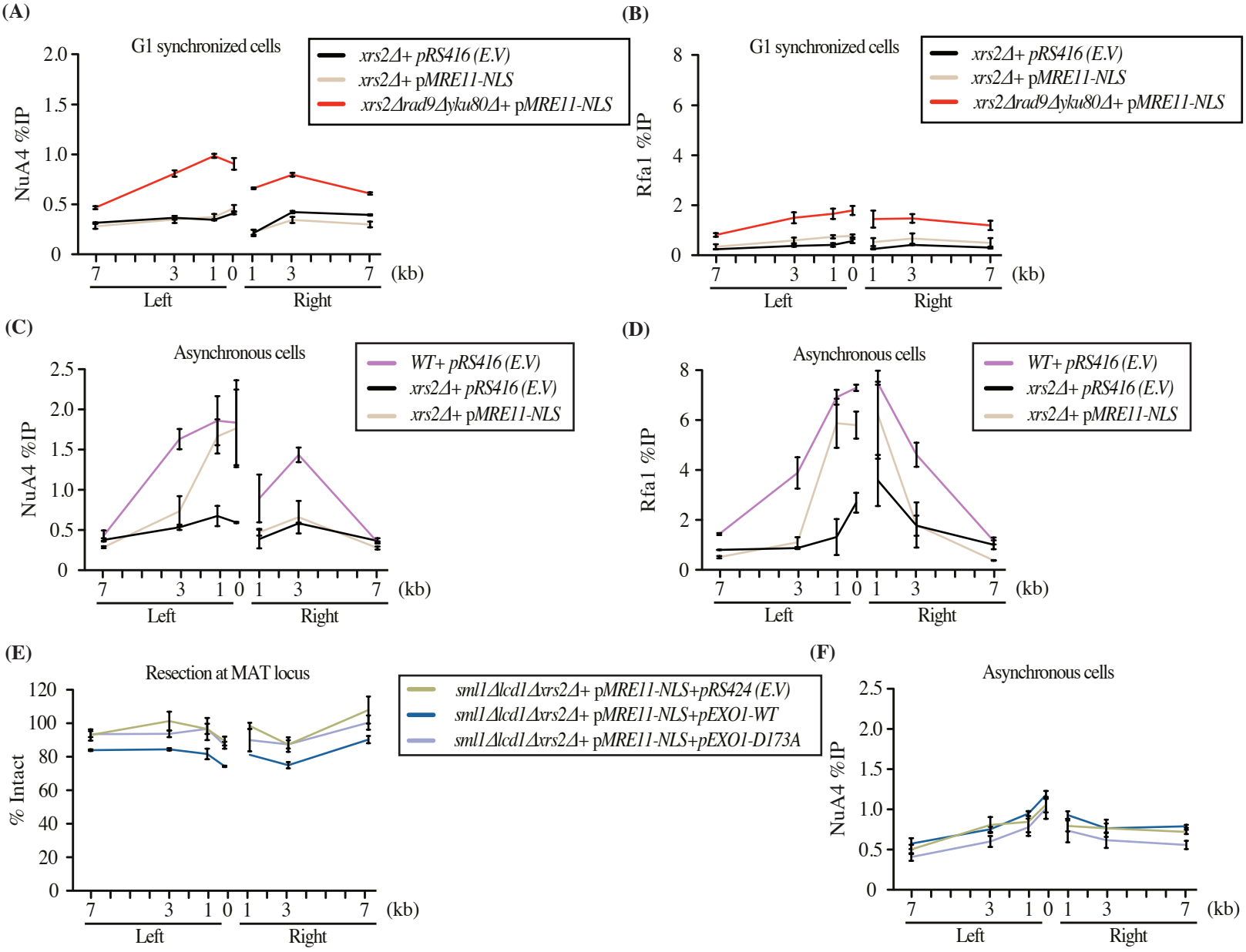
(A)
G1 synchronized cells
xrs2Δ+ pRS416 (E.V)
xrs2Δ+ pMRE11-NLS
xrs2Δrad9Δyku80Δ+ pMRE11-NLS
NuA4 %IP
2.0
1.5
1.0
0.5
0
7 3 1 0 1 3 7 (kb)
Left
Right
(B)
G1 synchronized cells
xrs2Δ+ pRS416 (E.V)
xrs2Δ+ pMRE11-NLS
xrs2Δrad9Δyku80Δ+ pMRE11-NLS
Rfa1 %IP
8
6
4
2
0
7 3 1 0 1 3 7 (kb)
Left
Right
(C)
Asynchronous cells
WT+ pRS416 (E.V)
xrs2Δ+ pRS416 (E.V)
xrs2Δ+ pMRE11-NLS
NuA4 %IP
2.5
2.0
1.5
1.0
0.5
0
7 3 1 0 1 3 7 (kb)
Left
Right
(D)
Asynchronous cells
WT+ pRS416 (E.V)
xrs2Δ+ pRS416 (E.V)
xrs2Δ+ pMRE11-NLS
Rfa1 %IP
8
6
4
2
0
7 3 1 0 1 3 7 (kb)
Left
Right
(E)
Resection at MAT locus
sml1Δlcd1Δxrs2Δ+ pMRE11-NLS+pRS424 (E.V)
sml1Δlcd1Δxrs2Δ+ pMRE11-NLS+pEXO1-WT
sml1Δlcd1Δxrs2Δ+ pMRE11-NLS+pEXO1-D173A
% Intact
120
100
80
60
40
20
0
7 3 1 0 1 3 7 (kb)
Left
Right
(F)
Asynchronous cells
NuA4 %IP
2.5
2.0
1.5
1.0
0.5
0
7 3 1 0 1 3 7 (kb)
Left
Right

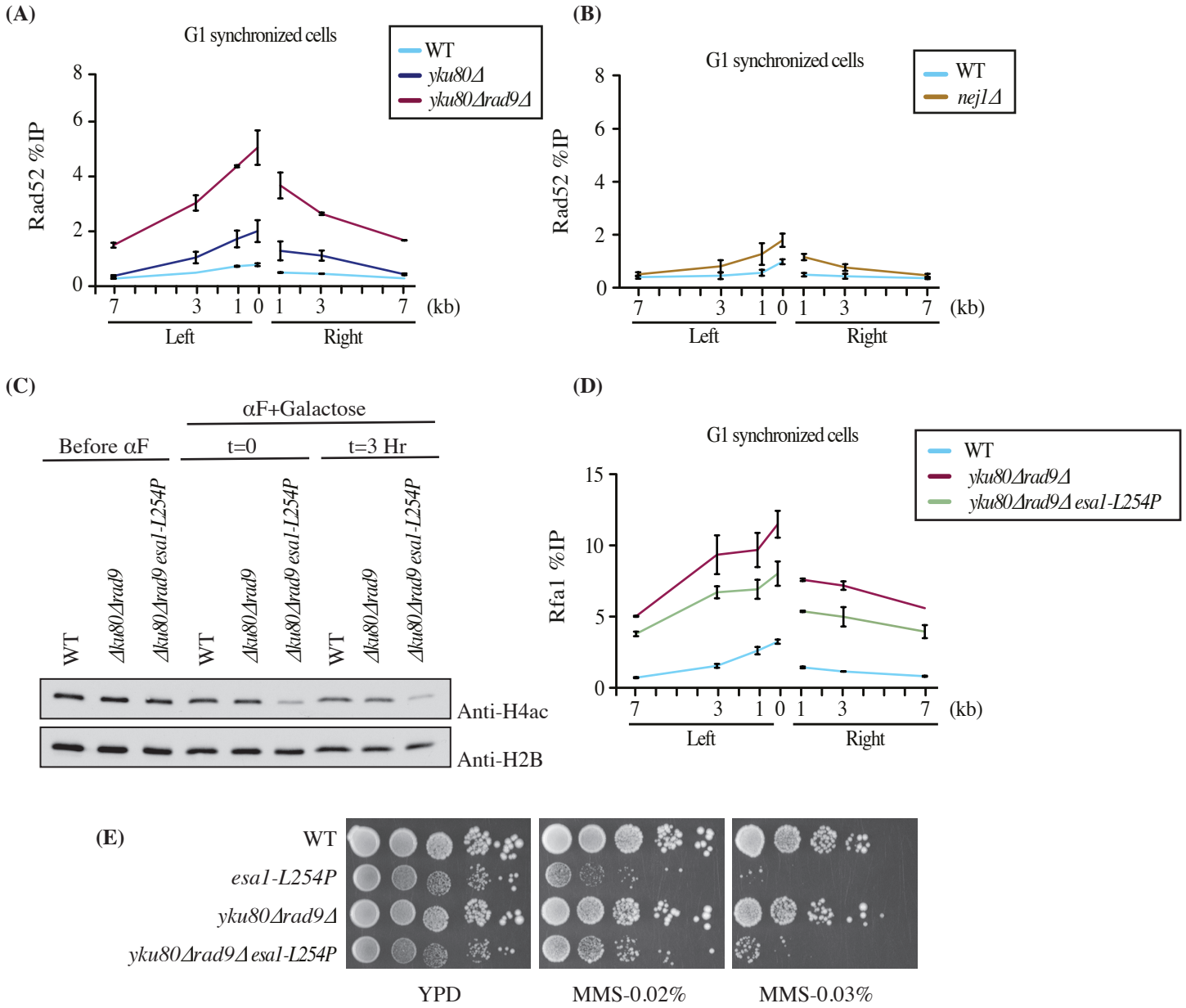
(A)
G1 synchronized cells
WT
yku80Δ
yku80Δrad9Δ
Rad52 %IP
8
6
4
2
0
7
3
1
0
1
3
7
(kb)
Left
Right
(B)
G1 synchronized cells
WT
nej1Δ
Rad52 %IP
8
6
4
2
0
7
3
1
0
1
3
7
(kb)
Left
Right
(C)
αF+Galactose
Before αF
t=0
t=3 Hr
WT
Δku80Δrad9
Δku80Δrad9 esa1-L254P
WT
Δku80Δrad9
Δku80Δrad9 esa1-L254P
WT
Δku80Δrad9
Δku80Δrad9 esa1-L254P
Anti-H4ac
Anti-H2B
(D)
G1 synchronized cells
WT
yku80Δrad9Δ
yku80Δrad9Δ esa1-L254P
Rfa1 %IP
15
10
5
0
7
3
1
0
1
3
7
(kb)
Left
Right
(E)
WT
esa1-L254P
yku80Δrad9Δ
yku80Δrad9Δ esa1-L254P
YPD
MMS-0.02%
MMS-0.03%

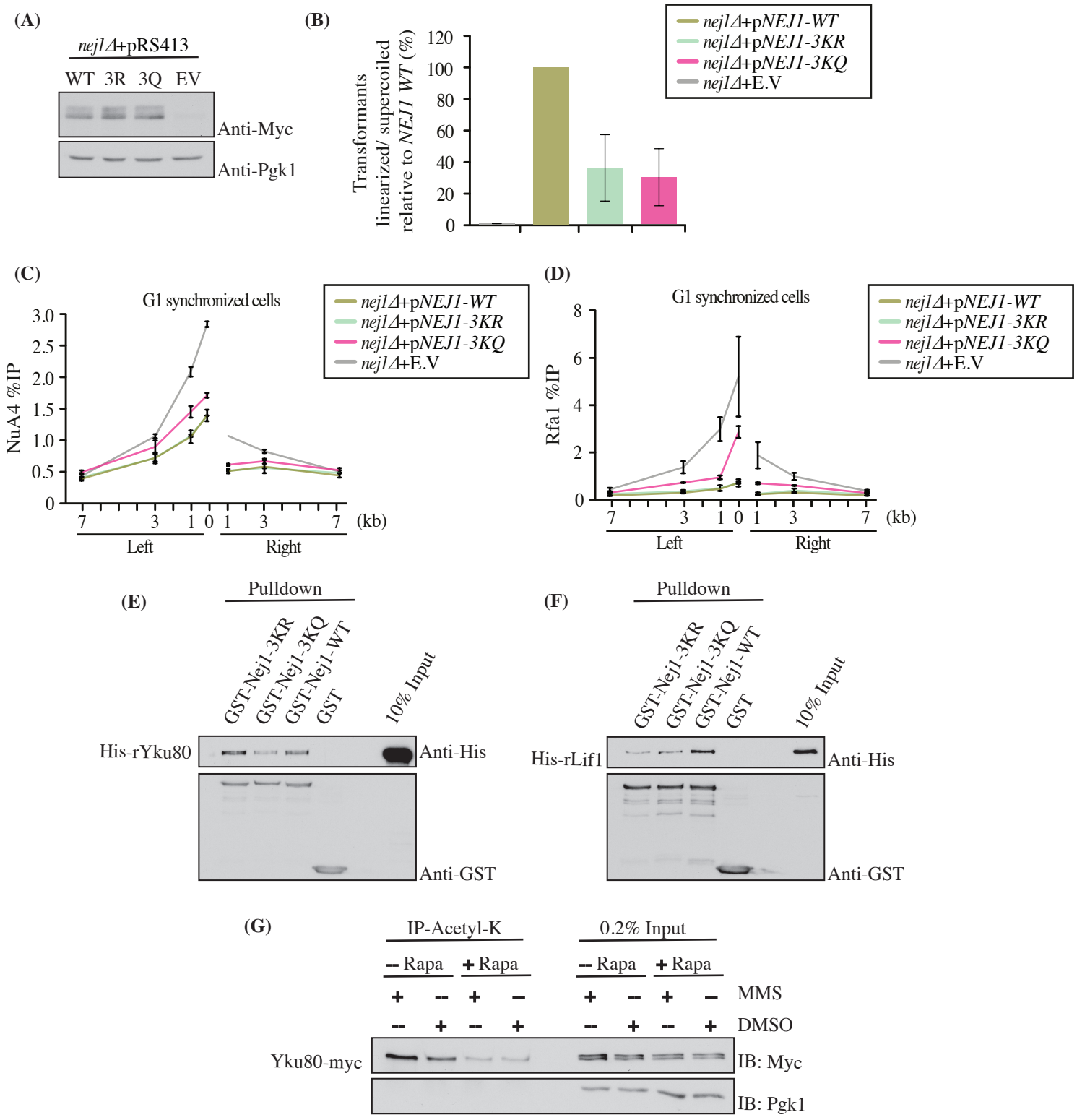
(A)
nej1Δ+pRS413
WT 3R 3Q EV
Anti-Myc
Anti-Pgk1
(B)
Transformants linearized/ supercoiled relative to NEJ1 WT (%)
120
100
80
60
40
20
0
nej1Δ+pNEJ1-WT
nej1Δ+pNEJ1-3KR
nej1Δ+pNEJ1-3KQ
nej1Δ+E.V
(C)
G1 synchronized cells
NuA4 %IP
3.0
2.5
2.0
1.5
1.0
0.5
0
7 3 1 0 1 3 7 (kb)
Left
Right
nej1Δ+pNEJ1-WT
nej1Δ+pNEJ1-3KR
nej1Δ+pNEJ1-3KQ
nej1Δ+E.V
(D)
G1 synchronized cells
Rfa1 %IP
8
6
4
2
0
7 3 1 0 1 3 7 (kb)
Left
Right
nej1Δ+pNEJ1-WT
nej1Δ+pNEJ1-3KR
nej1Δ+pNEJ1-3KQ
nej1Δ+E.V
(E)
Pulldown
GST-Nej1-3KR
GST-Nej1-3KQ
GST-Nej1-WT
GST
10% Input
His-rYku80
Anti-His
Anti-GST
(F)
Pulldown
GST-Nej1-3KR
GST-Nej1-3KQ
GST-Nej1-WT
GST
10% Input
His-rLif1
Anti-His
Anti-GST
(G)
IP-Acetyl-K
0.2% Input
– Rapa
+ Rapa
– Rapa
+ Rapa
+ – + – + – + –
MMS
– + – + – + – +
DMSO
Yku80-myc
IB: Myc
IB: Pgk1

FIGURE 6

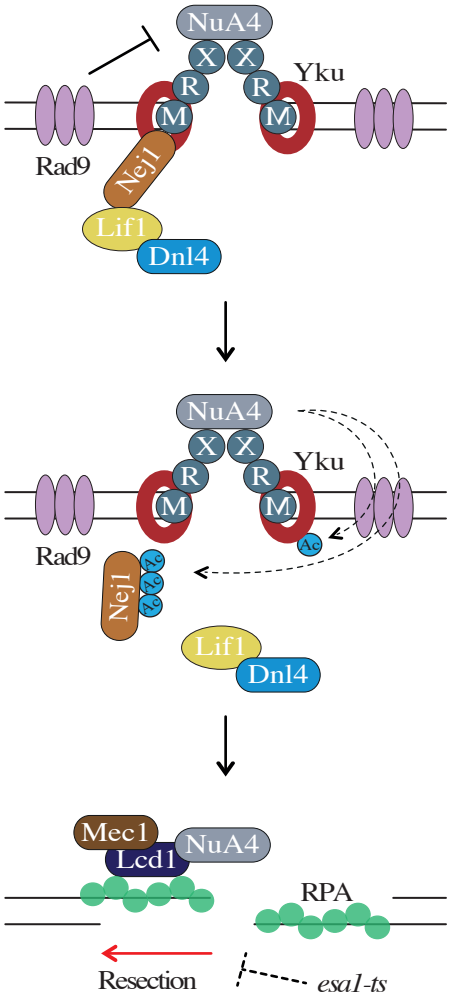
NuA4
X
X
R
R
M
M
Yku
Rad9
Nej1
Lif1
Dnl4
NuA4
X
X
R
R
M
M
Yku
Ac
Rad9
Nej1
Ac
Ac
Ac
Lif1
Dnl4
Mec1
Lcd1
NuA4
RPA
Resection
esa1-ts

S1 Fig.

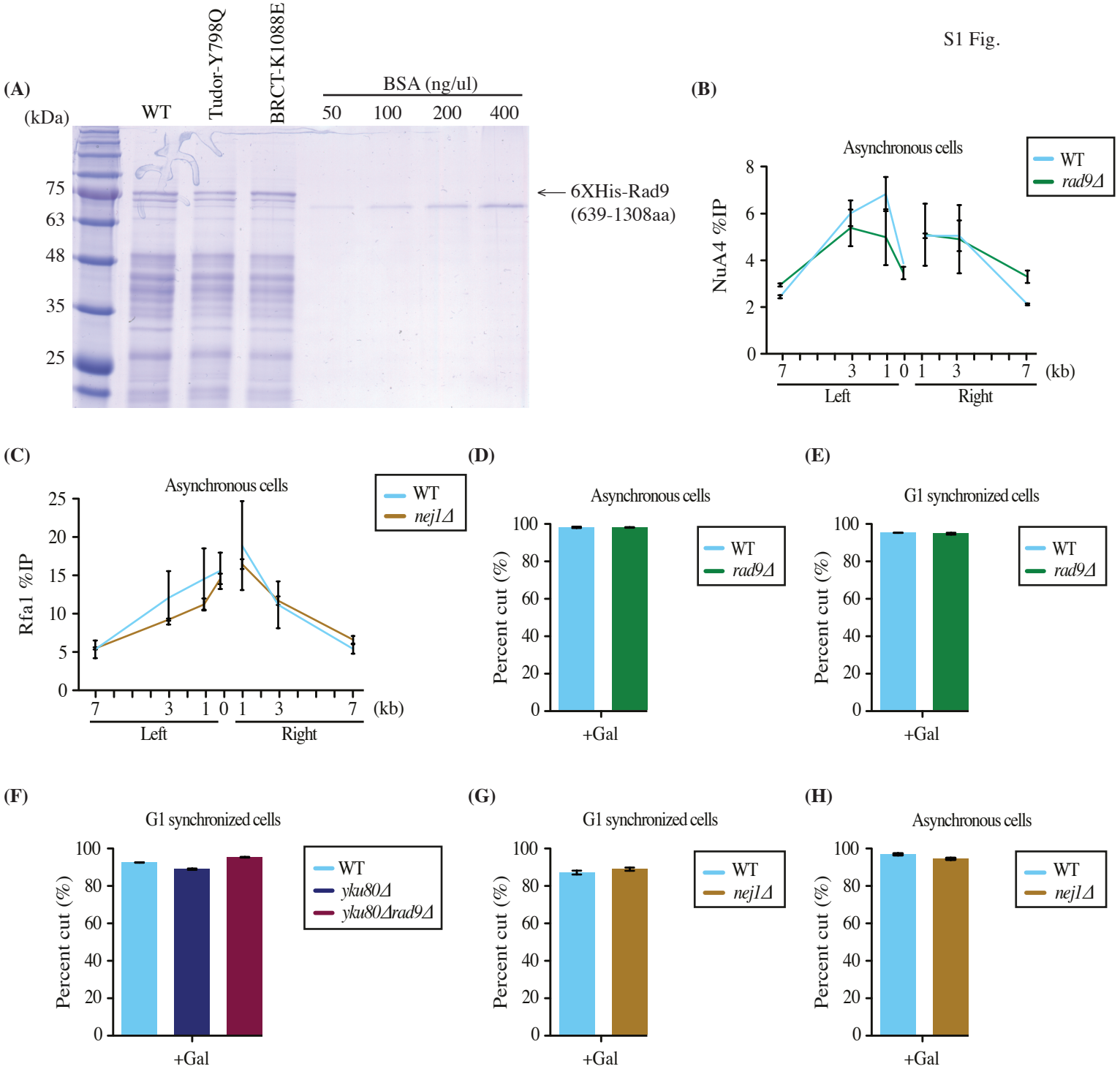
(A)
(kDa)
WT
Tudor-Y798Q
BRCT-K1088E
BSA (ng/ul)
50
100
200
400
75
63
48
35
25
6XHis-Rad9
(639-1308aa)
(B)
Asynchronous cells
WT
rad9Δ
NuA4 %IP
8
6
4
2
0
7
3
1
0
1
3
7
(kb)
Left
Right
(C)
Asynchronous cells
WT
nej1Δ
Rfa1 %IP
25
20
15
10
5
0
7
3
1
0
1
3
7
(kb)
Left
Right
(D)
Asynchronous cells
WT
rad9Δ
Percent cut (%)
100
80
60
40
20
0
+Gal
(E)
G1 synchronized cells
WT
rad9Δ
Percent cut (%)
100
80
60
40
20
0
+Gal
(F)
G1 synchronized cells
WT
yku80Δ
yku80Δrad9Δ
Percent cut (%)
100
80
60
40
20
0
+Gal
(G)
G1 synchronized cells
WT
nej1Δ
Percent cut (%)
100
80
60
40
20
0
+Gal
(H)
Asynchronous cells
WT
nej1Δ
Percent cut (%)
100
80
60
40
20
0
+Gal

S2 Fig.

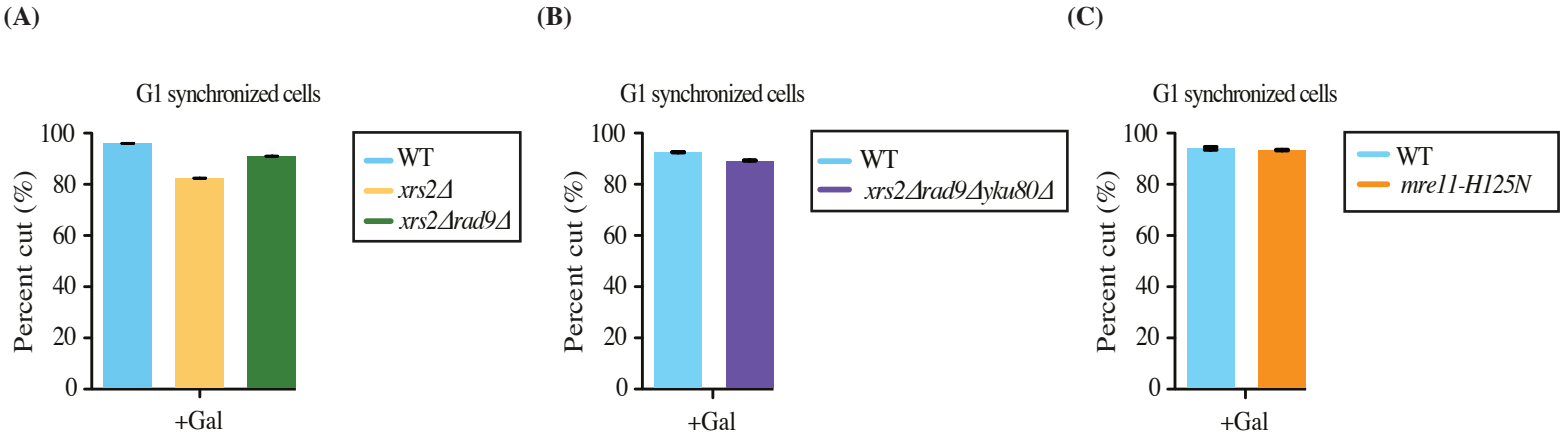
(A)
G1 synchronized cells
Percent cut (%)
100
80
60
40
20
0
+Gal
WT
xrs2Δ
xrs2Δrad9Δ
(B)
G1 synchronized cells
Percent cut (%)
100
80
60
40
20
0
+Gal
WT
xrs2Δrad9Δyku80Δ
(C)
G1 synchronized cells
Percent cut (%)
100
80
60
40
20
0
+Gal
WT
mre11-H125N

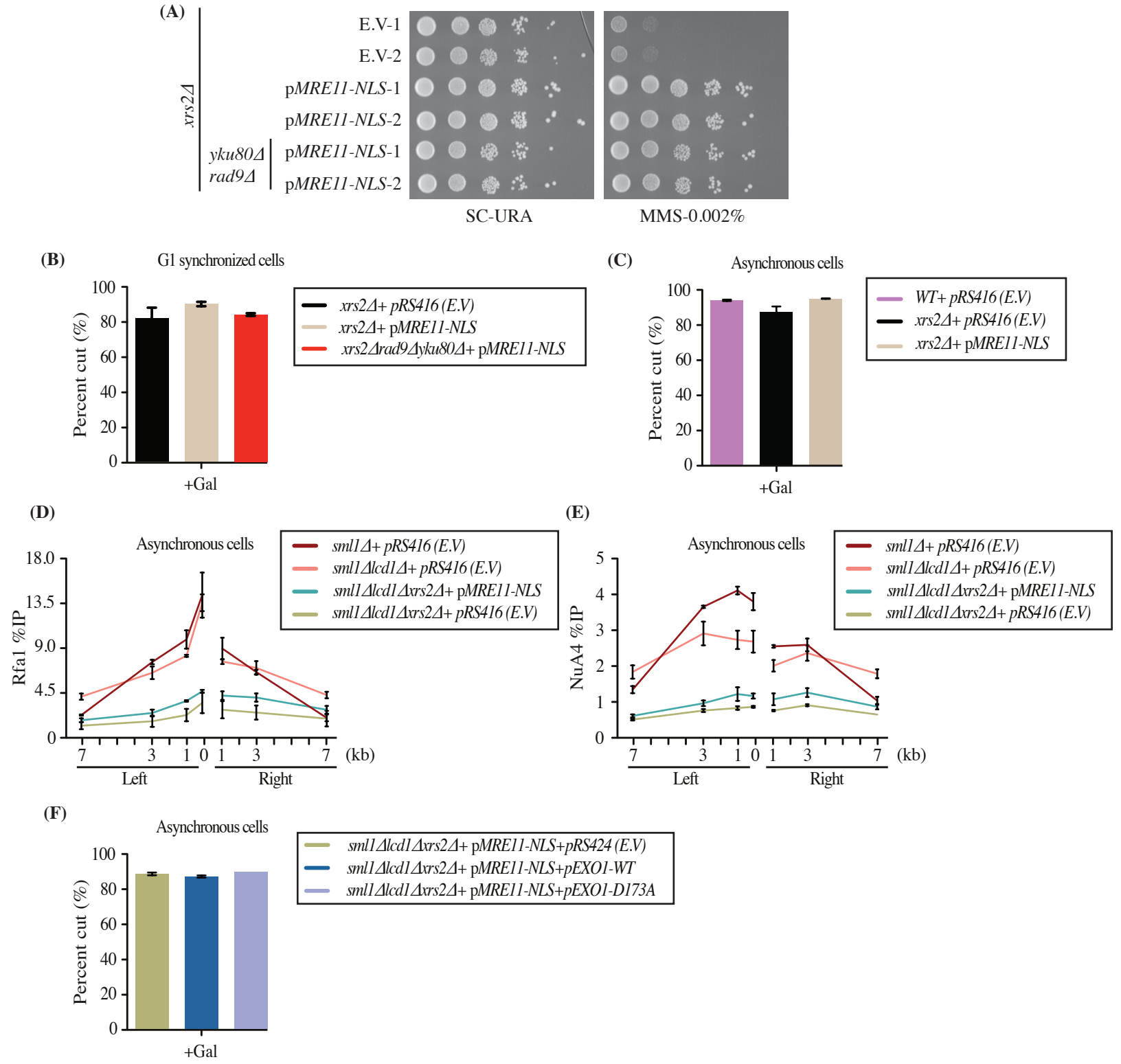
(A)
xrs2Δ
yku80Δ
rad9Δ
E.V-1
E.V-2
pMRE11-NLS-1
pMRE11-NLS-2
pMRE11-NLS-1
pMRE11-NLS-2
SC-URA
MMS-0.002%
(B)
G1 synchronized cells
Percent cut (%)
+Gal
xrs2Δ+ pRS416 (E.V)
xrs2Δ+ pMRE11-NLS
xrs2Δrad9Δyku80Δ+ pMRE11-NLS
(C)
Asynchronous cells
Percent cut (%)
+Gal
WT+ pRS416 (E.V)
xrs2Δ+ pRS416 (E.V)
xrs2Δ+ pMRE11-NLS
(D)
Asynchronous cells
Rfa1 %IP
Left
Right
(kb)
sml1Δ+ pRS416 (E.V)
sml1Δlcd1Δ+ pRS416 (E.V)
sml1Δlcd1Δxrs2Δ+ pMRE11-NLS
sml1Δlcd1Δxrs2Δ+ pRS416 (E.V)
(E)
Asynchronous cells
NuA4 %IP
Left
Right
(kb)
sml1Δ+ pRS416 (E.V)
sml1Δlcd1Δ+ pRS416 (E.V)
sml1Δlcd1Δxrs2Δ+ pMRE11-NLS
sml1Δlcd1Δxrs2Δ+ pRS416 (E.V)
(F)
Asynchronous cells
Percent cut (%)
+Gal
sml1Δlcd1Δxrs2Δ+ pMRE11-NLS+pRS424 (E.V)
sml1Δlcd1Δxrs2Δ+ pMRE11-NLS+pEXO1-WT
sml1Δlcd1Δxrs2Δ+ pMRE11-NLS+pEXO1-D173A

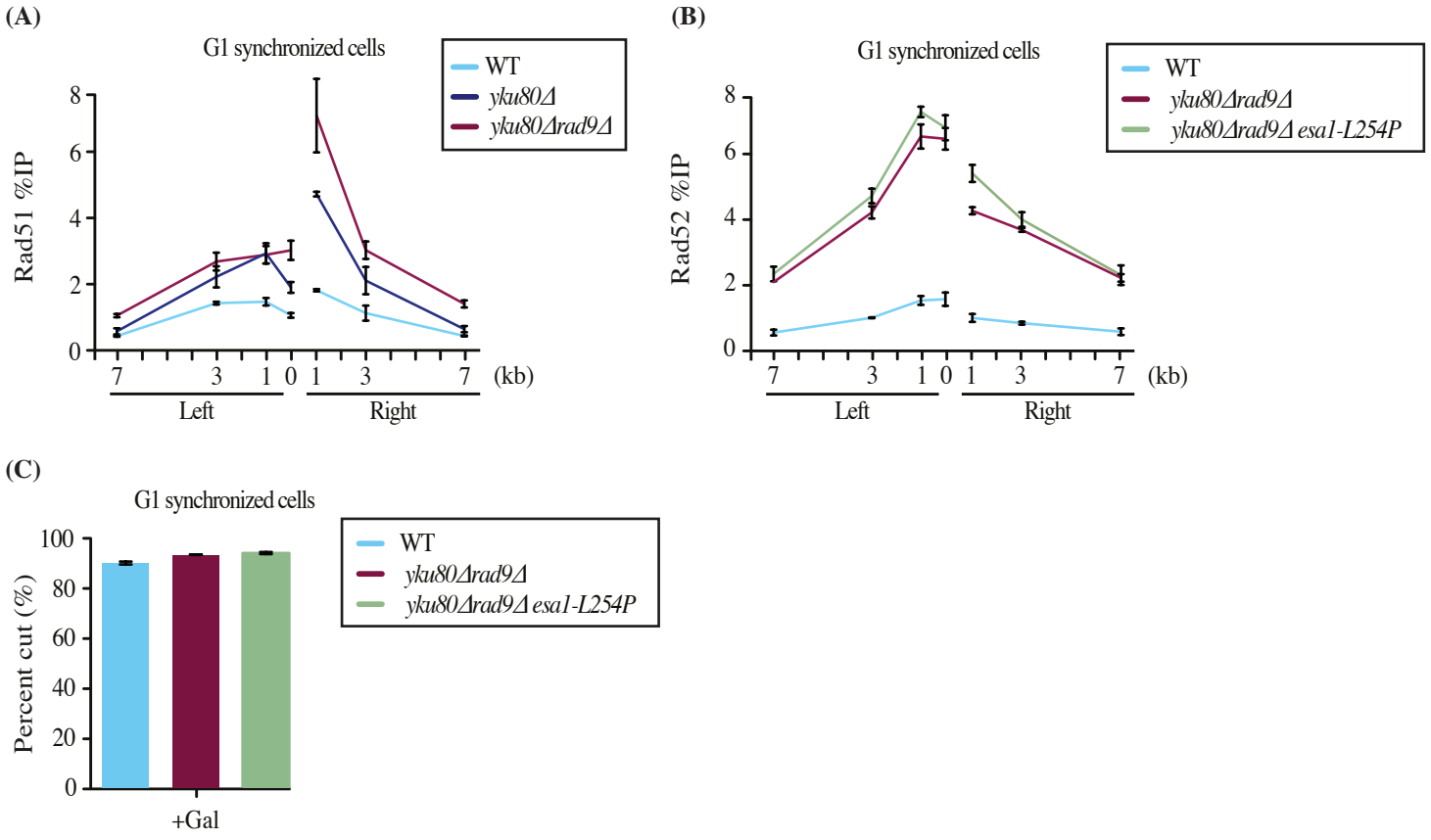
(A)
G1 synchronized cells
WT
yku80Δ
yku80Δrad9Δ
Rad51 %IP
0
2
4
6
8
7
3
1
0
1
3
7
(kb)
Left
Right
(B)
G1 synchronized cells
WT
yku80Δrad9Δ
yku80Δrad9Δ esa1-L254P
Rad52 %IP
0
2
4
6
8
7
3
1
0
1
3
7
(kb)
Left
Right
(C)
G1 synchronized cells
WT
yku80Δrad9Δ
yku80Δrad9Δ esa1-L254P
Percent cut (%)
0
20
40
60
80
100
+Gal

S5 Fig.

(A)

Ac-Nej1	
Esa1 -WT	*esa1 -ts*
K18	
K164	K164
K192	
K207	K207
K214	K214
K234	
K317	K317

(B)

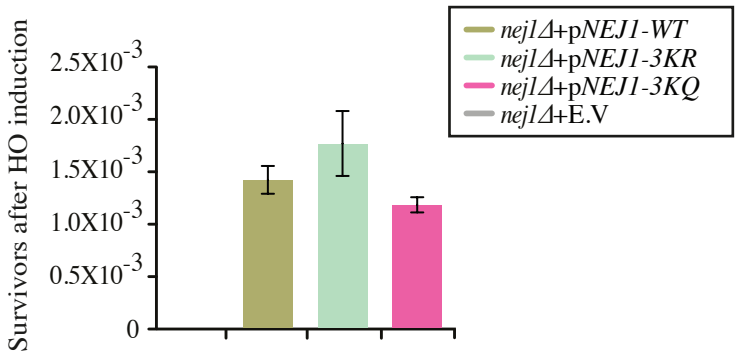

(C)

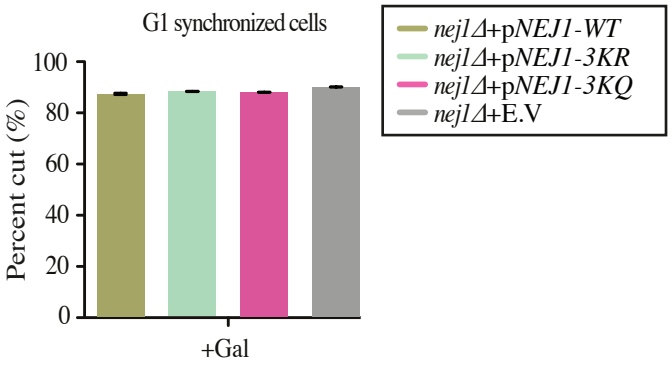

(D)

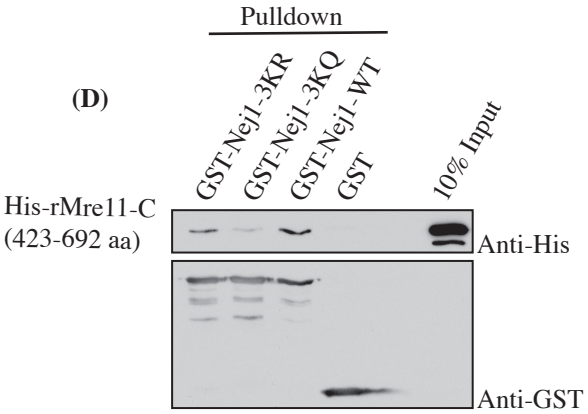

(E)

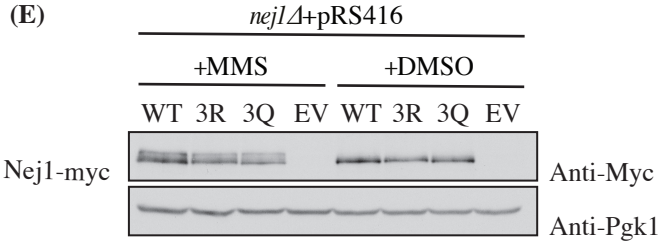

(F)

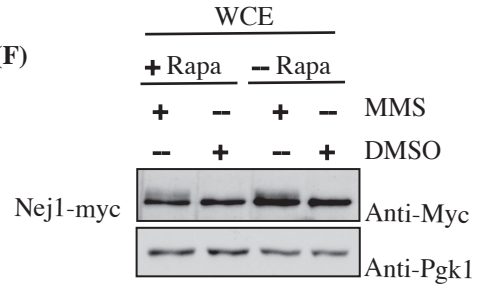
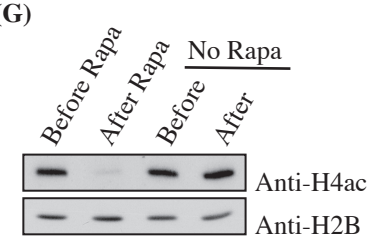
(G)